ARTICLE

doi:10.1038/nature20793

Piezo2 senses airway stretch and mediates lung inflation-induced apnoea

Keiko Nonomura[1]*, Seung-Hyun Woo[1]*, Rui B. Chang[2]*, Astrid Gillich[3], Zhaozhu Qiu[1,4]†, Allain G. Francisco[1], Sanjeev S. Ranade[1]†, Stephen D. Liberles[2] & Ardem Patapoutian[1]

Respiratory dysfunction is a notorious cause of perinatal mortality in infants and sleep apnoea in adults, but the mechanisms of respiratory control are not clearly understood. Mechanical signals transduced by airway-innervating sensory neurons control respiration; however, the physiological significance and molecular mechanisms of these signals remain obscured. Here we show that global and sensory neuron-specific ablation of the mechanically activated ion channel Piezo2 causes respiratory distress and death in newborn mice. Optogenetic activation of Piezo2$^+$ vagal sensory neurons causes apnoea in adult mice. Moreover, induced ablation of Piezo2 in sensory neurons of adult mice causes decreased neuronal responses to lung inflation, an impaired Hering–Breuer mechanoreflex, and increased tidal volume under normal conditions. These phenotypes are reproduced in mice lacking Piezo2 in the nodose ganglion. Our data suggest that Piezo2 is an airway stretch sensor and that Piezo2-mediated mechanotransduction within various airway-innervating sensory neurons is critical for establishing efficient respiration at birth and maintaining normal breathing in adults.

Respiratory organs experience repetitive and wide-ranging mechanical forces during breathing. On average, an adult man ventilates 0.5 l of air per breath and can inhale up to 3.5 l of air[1]. These mechanical forces within the airways are thought to serve as cues to trigger physiological responses[2,3]. However, the respiratory function of mechanotransduction is not well understood, partly owing to our inability to selectively modulate mechanotransduction. A potential respiratory role of mechanotransduction is illustrated by the Hering–Breuer inspiratory reflex: artificial inflation of lungs in anaesthetized animals induces immediate cessation of respiration (apnoea), which subsequently terminates further inspiration, presumably to prevent over-expansion of the lungs[2–4].

The airways are innervated by both vagal and spinal sensory neurons, whose cell bodies are located in the jugular (superior)–nodose (inferior) ganglia complex and thoracic dorsal root ganglia (DRG), respectively[5–7]. Although little is known about the function of somatic primary afferent neurons during respiration[7], the role of vagal innervation to the airway has been predominantly explored by denervation experiments and electrophysiological recordings of vagal nerves[3,5]. These studies have shown that vagal sensory neurons convey essential sensory information (for example, measurements of lung inflation, arterial oxygen pressure, and arterial pH) to the respiratory centre of the brainstem[2,3,5,6]. Vagotomized rats, for example, show dysregulated breathing characteristics such as a 1.7-fold increase in tidal volume (volume per breath) and a 2.4-fold decrease in breathing frequency in the absence of proper vagal sensory feedback[6,8]. Importantly, the Hering–Breuer reflex is mediated by vagal sensory neurons, although the underlying molecular mechanism of mechanotransduction by these neurons is unknown[2,3,5,6]. A recent study identified two distinct vagal sensory neuron subtypes that innervate the lung and have unique functions: activation of neurons expressing the purinergic receptor P2ry1 induces apnoea, whereas activation of neurons expressing the neuropeptide receptor Npy2r causes rapid, shallow breathing[9]. However, the stimulus (mechanical and/or chemical) that drives the firing of these neurons remains unknown.

At birth, our respiratory system undergoes striking structural changes as liquid-filled fetal lungs are inflated with air to allow efficient gas exchange[10]. This mechanical transformation is a critical and challenging process for newborns, and defects in this process are a notorious cause of perinatal mortality[10]. However, even less is known about the role of mechanotransduction in newborn respiration than in adult breathing[11]. Previous studies have suggested that vagal innervation is also critical for establishing newborn respiration, as vagotomized newborn lambs have unexpanded lungs and compromised breathing[12,13]. Whether these phenotypes are associated with impaired mechanotransduction in the airway is not clear, as vagal sensory neurons also detect a variety of chemicals[3].

Piezo2, a mechanically activated cation channel, is the principal mechanotransducer in low-threshold cutaneous mechanoreceptors and skeletal-muscle-innervating proprioceptors in mice[14–17]. On the basis of the function of Piezo2 as a mechanotransducer and its abundance in various populations of sensory neurons[9,15,18], we used Piezo2-deficient mouse models to investigate whether Piezo2-mediated mechanotransduction is involved in respiratory function.

Respiratory defects in *Piezo2*$^{-/-}$ mice

When Piezo2 was constitutively and globally ablated in mice, Piezo2-deficient (*Piezo2*$^{-/-}$) mice were born in the expected Mendelian ratio, but died within 24 h of birth[19] (Fig. 1a). Newborn *Piezo2*$^{-/-}$ pups showed signs of respiratory distress, such as cyanosis and gasping (Supplementary Information Video 1) and also failed to suckle (Fig. 1b). *Piezo2*$^{-/-}$ pups showed significantly decreased oxygen saturation levels (% SpO_2) in blood compared to their wild-type littermates (Fig. 1c). We examined the breathing activities of *Piezo2*$^{-/-}$ newborn mice by whole-body plethysmography and detected that respiratory frequency (breaths per minute) was significantly lower in *Piezo2*$^{-/-}$ pups than in their wild-type littermates (Fig. 1d, e). Moreover, in wild-type pups, each inspiration was immediately followed by the expiratory peak, but this breathing pattern was disrupted in *Piezo2*$^{-/-}$

[1]Howard Hughes Medical Institute, Molecular and Cellular Neuroscience, Dorris Neuroscience Center, The Scripps Research Institute, La Jolla, California 92037, USA. [2]Department of Cell Biology, Harvard Medical School, Boston, Massachusetts 02115, USA. [3]Howard Hughes Medical Institute, Department of Biochemistry, Stanford University School of Medicine, Stanford, California 94305, USA. [4]Genomics Institute of the Novartis Research Foundation, San Diego, California 92121, USA. †Present address: Department of Physiology and Solomon H. Snyder Department of Neuroscience, Johns Hopkins University School of Medicine, Baltimore, Maryland 21205, USA (Z.Q.); The Gladstone Institute, San Francisco, California 94158, USA (S.S.R.).
*These authors contributed equally to this work.

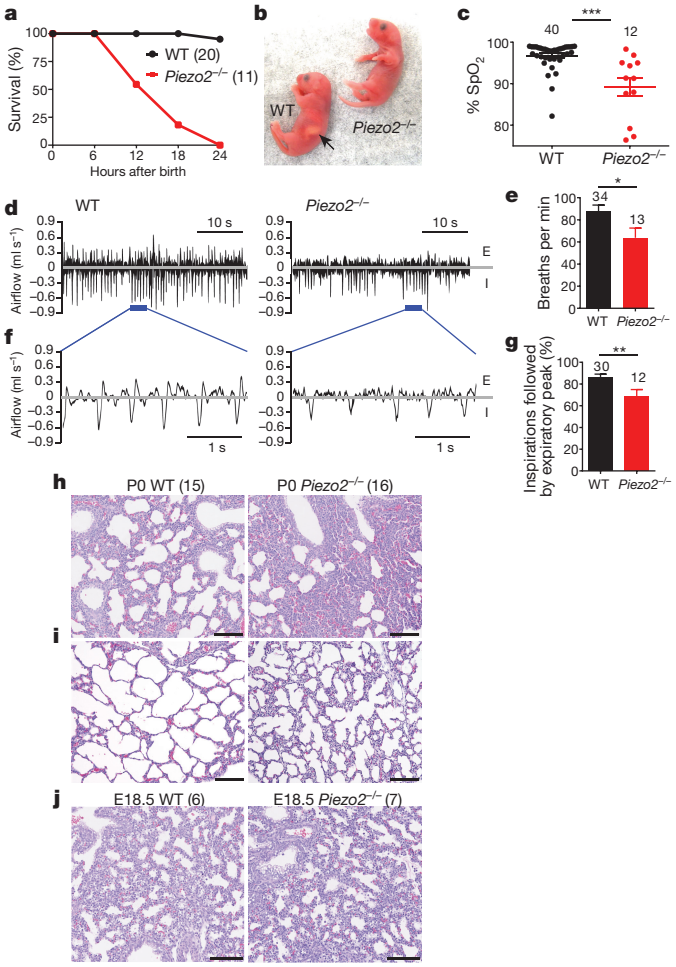

Figure 1 | Respiratory distress and lethality observed in *Piezo2*$^{-/-}$ newborn mice. a, Survival curve. WT, wild-type. **b**, A representative picture of newborn mice. Arrow indicates milk in the stomach. **c**, % SpO_2 in wild-type and *Piezo2*$^{-/-}$ newborn mice. ***$P < 0.001$, Mann–Whitney test. Bars represent mean ± s.e.m. **d**–**g**, Respiratory patterns. **d**, **f**, Representative traces of respiratory air flow (ml s^{-1}). E, expiration; I, inspiration. **e**, Breaths per min; **g**, per cent of inspirations followed by expiratory peak; *$P < 0.05$, **$P < 0.01$, unpaired Student's *t*-test, mean ± s.e.m. **h**–**j**, Haematoxylin and eosin staining of sections of the left lung. Lungs were isolated immediately after birth (**h**), about 6 h after birth (**i**), or at embryonic day (E)18.5 (**j**). Scale bars, 100 μm. Number of animals shown in parentheses.

pups (Fig. 1f, g). As these data suggest that respiration is compromised in *Piezo2*$^{-/-}$ mice, we performed histological characterization of the lungs of these mice. Haematoxylin and eosin staining of lung sections from *Piezo2*$^{-/-}$ mice revealed substantially reduced airspaces throughout all lobes compared to wild-type lungs (Fig. 1h, i). This phenotype was consistently observed in all *Piezo2*$^{-/-}$ pups from independent litters. We investigated whether respiratory complications in *Piezo2*$^{-/-}$ newborn mice were caused by Piezo2 ablation during prenatal lung development[10,20], but found no defects in embryonic lung anatomy, pneumocyte differentiation, or clearance of the fetal pulmonary fluid in *Piezo2*$^{-/-}$ embryos or newborn mice (Fig. 1j, Extended Data Fig. 1). Collectively, these results suggest that *Piezo2*$^{-/-}$ mice develop normally but show signs of respiratory failure after birth.

Piezo2 expression in the respiratory system

The respiratory system involves various tissues, such as the brainstem, airway tract and lungs, sensory and autonomic nervous systems, motor neurons, and respiratory muscles. To investigate how ablation of Piezo2 disrupts respiration, we first assessed Piezo2 expression in the respiratory system using the previously described *Piezo2–GFP-IRES-Cre* (*Piezo2*^{GFP}) reporter line[21] (Extended Data Fig. 2). *Piezo2*^{GFP} reporter mice express the Piezo2–GFP (green fluorescent protein) fusion protein as well as Cre recombinase through an internal ribosome entry site (IRES) under the *Piezo2* promoter. Within the airway tract of these mice, we detected GFP expression in pulmonary neuroepithelial cell bodies (NEBs) but not in other cell types of the lung (Extended Data Fig. 2a). NEBs have been proposed to function as oxygen sensors, mechanosensors, and chemosensors of the airway, but their exact role remains unclear[3,22,23]. We also detected GFP expression in neuronal cells of the jugular–nodose ganglia complex, trigeminal ganglia and thoracic DRG[9,15,16] (Extended Data Fig. 2b–e). However, we did not detect GFP expression in respiratory control centres of the brainstem, the dorsal nucleus of the vagus nerve, motor neurons in the spinal cord, sympathetic ganglia, diaphragm or intercostal muscles[6,10,24] (Extended Data Fig. 2f–k). In addition to the respiratory system, we also examined GFP expression in other major organs that might indirectly affect respiration, including the heart, liver and kidneys. However, we did not detect GFP expression in these organs (data not shown). We also crossed the *Piezo2*^{GFP} mouse line with the tdTomato reporter line (*Ai9*) and generated *Piezo2*^{GFP}*;Ai9* mice because tdTomato, which is highly expressed after Cre-mediated recombination can serve as a more sensitive detection method than GFP immunostaining. It is important to note that this is a lineage tracing method; therefore, even cells that transiently expressed Piezo2 during development would be permanently labelled with tdTomato. In *Piezo2*^{GFP}*;Ai9* mice, tdTomato was present in pulmonary NEBs, vagal and spinal sensory neurons, and endothelial cells in various tissues (Extended Data Fig. 3). Collectively, our two reporter studies suggest that Piezo2 is expressed in pulmonary NEBs, vagal and spinal sensory neurons, and possibly all endothelial cells (Extended Data Fig. 2l).

Tissue-specific *Piezo2* cKO mouse lines

To investigate which Piezo2-expressing cell types contribute to *Piezo2*$^{-/-}$ lethality and respiratory distress, we generated *Piezo2* conditional knockout (cKO) mice using various tissue-specific Cre mouse lines (Table 1). To eliminate Piezo2 in all endothelial cells, we crossed *Tie2Cre* (*Tie2* is also known as *Tek*) mice with *Piezo2*$^{fl/fl}$ mice to generate *Tie2Cre;Piezo2*^{cKO} mice[21,25] (Extended Data Figs 4a–e, 5a). *Tie2Cre;Piezo2*^{cKO} mice survived to adulthood without displaying any health complications (Table 1). Characterization of newborn mice showed that *Tie2Cre;Piezo2*^{cKO} and wild-type pups had comparable % SpO_2 and lung morphology (Fig. 2a, b). These results suggest that ablation of Piezo2 in endothelial cells is not sufficient to cause the respiratory complications and lethality seen in *Piezo2*$^{-/-}$ mice.

Table 1 | Summary of tissue-specific *Piezo2* conditional knockout mouse characterization

Tissue-specific *Cre* mouse	Cre expression						Survival of *Piezo2* cKO at birth
	ECs	NEB	Nodose	Jugular	Trigeminal	DRG	
Tie2Cre	Yes	No	No	No	No	No	Yes
Phox2bCre	No	No	Yes	No	No	No	Yes
Wnt1Cre	No	No	No	Yes	Yes	Yes	No
AdvillinCreER^{T2+Tam}	No	No	Yes	Yes	Yes	Yes	KD induced in adults

ECs, endothelial cells. KD, knockdown. Ratios of *Piezo2* cKO mice derived from crosses between various *Cre;Piezo2*$^{+/-}$ and *Piezo2*$^{fl/fl}$ mice: *Tie2Cre;Piezo2*^{cKO} mice, 15/59 (25.4%); *Phox2bCre;Piezo2*^{cKO} mice, 17/51 (33.3%) at 3 weeks after birth; *Wnt1Cre;Piezo2*^{cKO} mice, 9/34 (26.4%) at postnatal day 0, 0/25 (0%) at postnatal day 1.

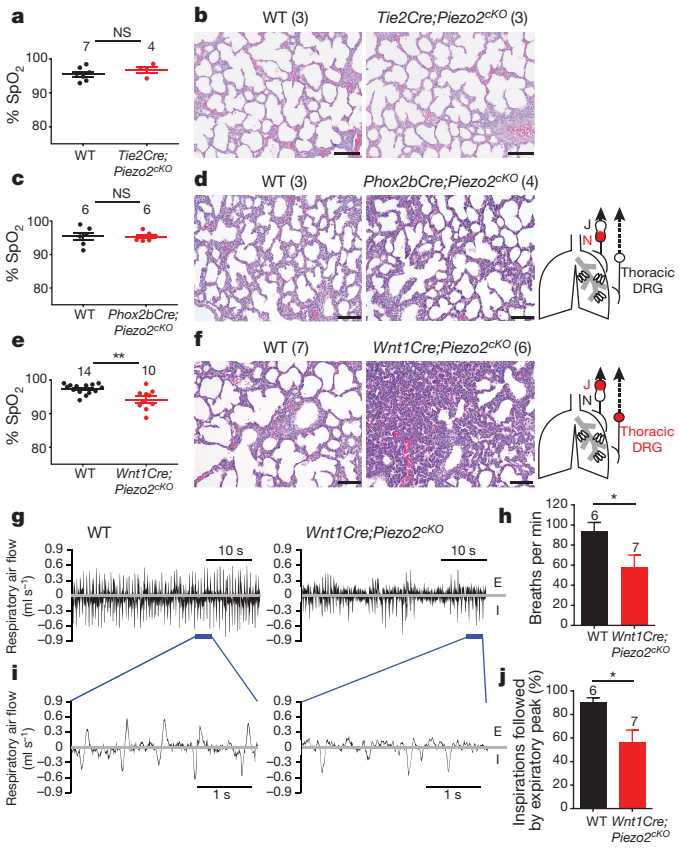

Figure 2 | Characterization of tissue-specific *Piezo2* conditional knockout (cKO) mice. a, **b**, *Tie2Cre;Piezo2*^{cKO} newborn mice. **c**, **d**, *Phox2bCre;Piezo2*^{cKO} newborn mice. **e**–**j** *Wnt1Cre;Piezo2*^{cKO} newborn mice. **a**, **c**, **e**, % SpO_2. $^{**}P < 0.01$, Mann–Whitney test. NS, statistically not significant. Bars represent mean ± s.e.m. **b**, **d**, **f**, Haematoxylin and eosin staining of sections of the left lung. Right panels in **d** and **f** show Piezo2-depleted tissues in red. J, jugular ganglion. N, no-dose ganglion. **g**, **i**, Representative traces of respiratory air flow (ml s^{-1}). **h**, Breaths per minute. **j**, Per cent of inspirations followed by expiratory peak. $^{*}P < 0.05$, unpaired Student's (**h**) or Welch's (**j**) *t*-test, mean ± s.e.m. All scale bars, 100 μm. Number of animals shown in parentheses.

Next, we ablated Piezo2 in vagal and spinal sensory neurons by using two independent Cre lines: *Phox2bCre* and *Wnt1Cre*[26,27]. The *Phox2bCre* line targets Piezo2 in nodose ganglia, which are derived from epibranchial placodes, whereas the *Wnt1Cre* line targets Piezo2 in jugular, trigeminal and dorsal root ganglia, all of which are derived from the neural crest[5,28,29] (Table 1, Extended Data Figs 4f–m, 5b, c). *Phox2bCre;Piezo2*^{cKO} mice also survived to adulthood (Table 1), and *Phox2bCre;Piezo2*^{cKO} and wild-type newborn mice showed comparable % SpO_2 and lung structure (Fig. 2c, d). These results indicate that Piezo2 in nodose ganglia is not, by itself, required to establish adequate respiration at birth and that its absence does not lead to the lethality seen in *Piezo2*$^{-/-}$ mice. By contrast, *Wnt1Cre;Piezo2*^{cKO} newborn mice died within 24 h of birth (Table 1). Like newborn *Piezo2*$^{-/-}$ mice, *Wnt1Cre;Piezo2*^{cKO} pups showed signs of respiratory distress, such as cyanosis and gasping, and also failed to suckle (Supplementary Information Video 2), and their % SpO_2 was lower than that of wild-type littermates (Fig. 2e). Histological examination of the lungs of *Wnt1Cre;Piezo2*^{cKO} mice also revealed smaller airspaces than in wild-type lungs (Fig. 2f). On the basis of their phenotypes, we performed whole-body plethysmograph recordings in *Wnt1Cre;Piezo2*^{cKO} mice. In parallel to the respiratory patterns observed in *Piezo2*$^{-/-}$ mice, *Wnt1Cre;Piezo2*^{cKO} mice also showed reduced respiratory frequency and a significantly lower percentage of inspirations followed by the expiratory peak compared to wild-type littermates (Fig. 2g–j).

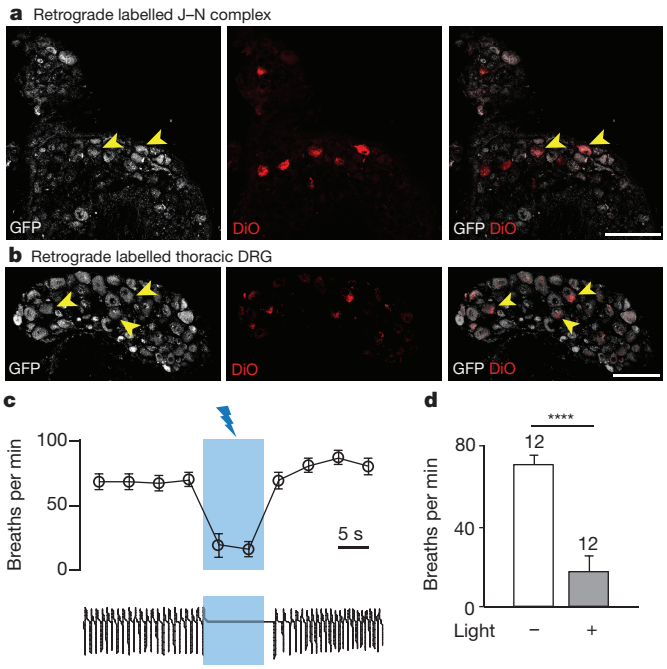

Figure 3 | Characterization of Piezo2^{+} vagal sensory neurons. a, **b**, GFP immunostaining in the jugular–nodose (J–N) ganglia complex (**a**) and thoracic DRG (**b**) of *Piezo2*^{GFP} reporter mice injected with DiO retrograde tracer into the lower tracheal lumen. Yellow arrowheads mark GFP^{+} DiO^{+} cells. Samples from four mice were analysed. Scale bars, 100 μm. **c**, Respiratory responses to focal illumination (blue shading) of the vagus nerve in *Piezo2*^{GFP}*;lox-ChR2* mice. Respiratory rhythms (representative traces, bottom) were measured by recording tracheal pressure. **d**, Light-induced changes in breathing rate over 10-s trial. $^{****}P < 0.0001$, unpaired Student's *t*-test, mean ± s.e.m.

Airway-innervating Piezo2^{+} neurons

To elucidate the role of Piezo2^{+} sensory neurons in respiration, we investigated whether Piezo2^{+} sensory neurons innervate the airway organs in adult mice. The presence of tdTomato^{+} nerve fibres innervating NEBs in the lungs of *Piezo2*^{GFP}*;Ai9* mice indicated that Piezo2 is expressed in airway-innervating sensory neurons at least during development (Extended Data Fig. 3b). To test whether Piezo2 is expressed in respiratory sensory neurons of adult mice, we performed retrograde labelling of airway-innervating sensory neurons by injecting octadecyl (C_{18})-oxycarbocyanine (DiO) into the bottom of the trachea of adult *Piezo2*^{GFP} mice to label sensory terminals innervating the trachea and/or the lungs[28]. GFP^{+} DiO^{+} neurons were detected in both the jugular–nodose ganglia complex and the thoracic DRG, suggesting that Piezo2 is indeed expressed in adult vagal and spinal sensory neurons that innervate the airway (Fig. 3a, b).

We next characterized the physiological function of airway-innervating Piezo2^{+} sensory neurons. We crossed *Piezo2*^{GFP} mice with Cre-dependent *channelrhodopsin-2 (lox-ChR2)* reporter mice to generate *Piezo2*^{GFP}*;lox-ChR2* mice, and tested the consequences of activating Piezo2^{+} vagal sensory neurons using optogenetics[9]. Airway-innervating vagal sensory neurons contain a mixed population of fast-conducting myelinated A fibres and slow-conducting unmyelinated C fibres[5]. Brief optogenetic stimulation (0.8 ms) of the vagal nerve trunk of *Piezo2*^{GFP}*;lox-ChR2* mice caused a compound action potential firing, consisting primarily of A-fibre responses (11.6 ± 4.7 m s^{-1}) and some C-fibre responses (0.68 ± 0.11 m s^{-1}) (Extended Data Fig. 6a, b). The current generated by selective stimulation of Piezo2^{+} vagal fibres was predominantly, but not exclusively, fast-conducting. In this experiment we potentially activated sensory neurons that transiently expressed Piezo2 during development as well as those that express Piezo2 in adult mice. We also characterized Piezo2^{+} vagal sensory neurons by isolating the jugular–nodose ganglia complex from adult

Piezo2^{GFP} reporter mice and immunostaining it with the A- and C-fibre markers Nefh and IB4, respectively[30,31]. Consistent with Piezo2 expression in both A- and C-fibres, subpopulations of GFP$^+$ neurons co-localized with either Nefh or IB4 (Extended Data Fig 6c, d).

Strikingly, longer optogenetic stimulation (10 s, 50 Hz) of the vagal nerve trunk caused immediate apnoea that lasted through the entire stimulation period and resulted in a decrease in the average breathing rate of about 75% when compared to the unstimulated rate (Fig. 3c, d). During optogenetic stimulation, the respiration of *Piezo2*^{GFP}*;lox-ChR2* mice was trapped in a state of exhalation based on their lung volume at apnoea (Extended Data Fig. 6e–g). Breathing activities returned to normal after optogenetic stimulation was removed (Fig. 3c). These data show that Piezo2$^+$ vagal sensory neurons innervate the airway organs and modulate respiration by inducing a respiratory block in a similar manner as previously described for P2ry1$^+$ vagal neurons[9]. This is not surprising, as a large number of P2ry1$^+$ neurons also express Piezo2 (ref. 9).

We also investigated how inputs from Piezo2$^+$ vagal sensory neurons are organized centrally. Infection of the jugular–nodose ganglia complex with *AAV-flex-tdTomato* in adult *Piezo2*^{GFP} mice yielded *tdTomato*$^+$ neuronal fibres in the nucleus of the solitary tract (NTS), the respiratory centre that is innervated by vagal sensory neurons[9] (Extended Data Fig. 6h).

Piezo2 is an airway stretch receptor

To test whether Piezo2 functions as a mechanotransducer in airway-innervating sensory neurons directly, we performed *in vivo* vagal sensory nerve recordings in adult sensory neuron-specific *Piezo2* conditional knockout mice. We used the previously described *AdvillinCreER*^{T2}*;Piezo2*^{cKO} mice to ablate Piezo2 in the majority of vagal and spinal sensory neurons in adult mice[15] (Extended Data Fig. 7a–d and Table 1). We inflated the lungs of the mice by injecting air through their tracheae and simultaneously measured vagal sensory nerve responses. *AdvillinCreER*^{T2}*;Piezo2*^{cKO} mice showed greatly reduced vagal nerve firing in response to lung inflation when compared to wild-type mice (Fig. 4a). These data provide direct evidence that Piezo2 functions as a key stretch transducer of airway-innervating vagal neurons.

We next tested whether ablation of Piezo2 in sensory neurons would affect normal breathing in adult mice. We compared respiratory

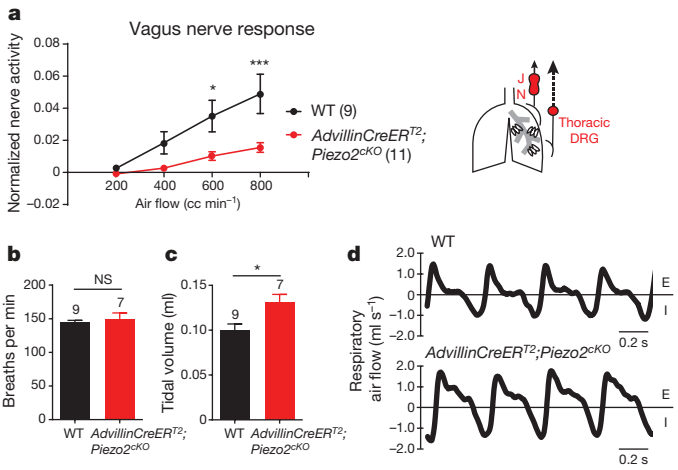

Figure 4 | Respiratory characteristics in adult *AdvillinCreER*^{T2}*;Piezo2*^{cKO} mice. a, Left, whole vagus nerve recording during lung inflation. Repeated measures two-way ANOVA: genotype $F_{(1,18)} = 8.077$, $P = 0.0108$; air flow $F_{(3,54)} = 28.62$, $P < 0.0001$; interaction $F_{(3,54)} = 6.372$, $P = 0.0009$. $^*P < 0.05$, $^{***}P < 0.001$, Sidak's post-hoc test; mean ± s.e.m. Right, Piezo2-depleted tissues shown in red. **b**–**d**, Whole-body plethysmograph recordings under anaesthesia. Average frequency (**b**) and average tidal volume (**c**); $^*P < 0.05$, unpaired Welch's (**b**) or Student's (**c**) *t*-test, mean ± s.e.m. **d**, Representative traces of respiratory air flow. E, expiration; I, inspiration. Number of animals shown in parentheses.

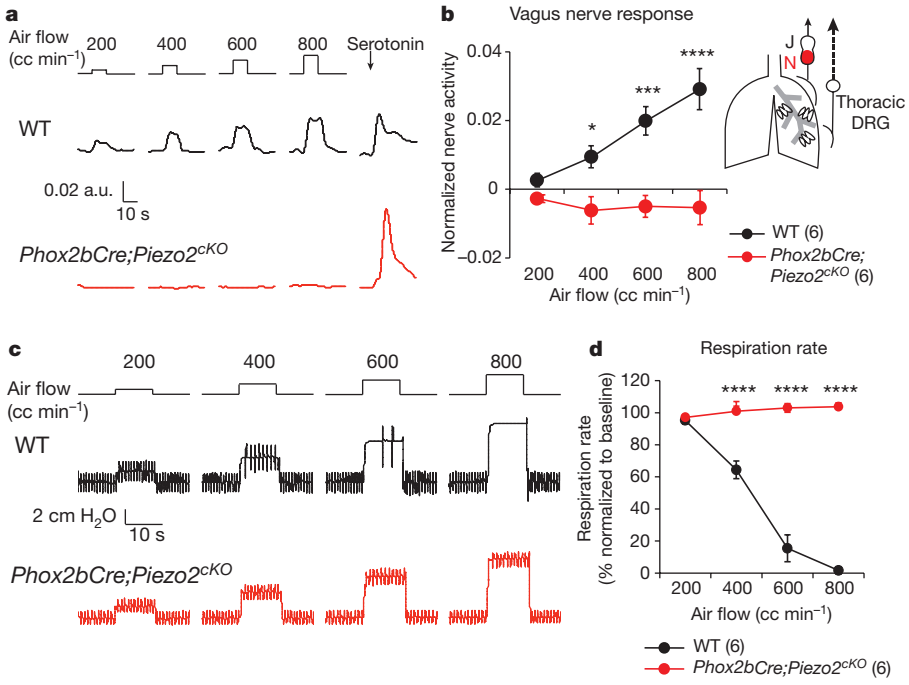

Figure 5 | Impaired detection of lung inflation in adult *Phox2bCre;Piezo2*^{cKO} mice. a, **b**, Whole vagus nerve recordings. **a**, Representative traces; **b**, Normalized nerve activity (mean ± s.e.m.). Repeated measures two-way ANOVA: genotype $F_{(1,10)} = 18.93$, $P = 0.0014$; air flow $F_{(3,30)} = 10.75$, $P < 0.0001$; interaction $F_{(3,30)} = 13.94$, $P < 0.0001$. $^*P < 0.05$, $^{***}P < 0.001$, $^{****}P < 0.0001$, Sidak's post-hoc test. Piezo2-depleted tissues shown in red (**b**, right). **c**, **d**, Respiratory patterns during lung inflation. **c**, Representative traces of tracheal pressure. Steps indicate induced pressure increases and each deflection is a breath. **d**, Normalized respiration rate (mean ± s.e.m.). Repeated measures two-way ANOVA: genotype $F_{(1,10)} = 188.7$, $P < 0.0001$; air flow $F_{(3,30)} = 97.48$, $P < 0.0001$; interaction $F_{(3,30)} = 126.4$, $P < 0.0001$, $^{****}P < 0.0001$, Sidak's post-hoc test. Number of animals shown in parentheses.

parameters measured by whole-body plethysmograph recordings in *AdvillinCreER^{T2};Piezo2^{cKO}* and wild-type mice (Fig. 4b–d, Extended Data Table 1). *AdvillinCreER^{T2};Piezo2^{cKO}* mice showed a 1.3-fold increase in tidal volume compared to wild-type littermates (Fig. 4c and Extended Data Table 1), which is similar to the tidal volume change observed in vagotomized adult mammals[6,8]. The increased tidal volume in *AdvillinCreER^{T2};Piezo2^{cKO}* mice suggests that lung volume changes are not precisely detected, and that *AdvillinCreER^{T2};Piezo2^{cKO}* mice are likely to breathe in excess air compared to wild-type littermates. By contrast, breathing frequency was normal in *AdvillinCreER^{T2};Piezo2^{cKO}* mice (Fig. 4b), whereas vagotomized adult mice and other mammals show reduced breathing frequency[6,8,32]. This difference suggests that other sensory inputs besides Piezo2-mediated mechanotransduction might be responsible for controlling breathing frequency. Moreover, there was a strong trend towards decreased duration of pause before inspiration in *AdvillinCreER^{T2};Piezo2^{cKO}* mice, resulting in a prolonged duration of expiratory air flow ($P = 0.08$; Fig. 4d upper peak traces, Extended Data Table 1). Our data show that Piezo2-mediated mechanotransduction is required for normal breathing in adult mice.

Previous studies have suggested that vagal sensory neurons in the nodose ganglia are the main source of low-threshold mechanosensors innervating the lower airway organs[5,28,33]. On the basis of our observations in *AdvillinCreER^{T2};Piezo2^{cKO}* mice, we investigated whether Piezo2 serves as the low-threshold mechanotransducer in nodose sensory neurons by assaying inflation-dependent vagal neuronal activity and normal respiratory activity in adult *Phox2bCre;Piezo2^{cKO}* mice. The vagal nerve response to lung inflation was abolished in *Phox2bCre;Piezo2^{cKO}* mice (Fig. 5a, b), indicating that Piezo2 functions as the major stretch sensor to detect lung inflation in the vagus nerve. *AdvillinCreER^{T2};Piezo2^{cKO}* mice showed a slightly milder effect on inflation-induced vagal activity than did *Phox2bCre;Piezo2^{cKO}* mice, and this might be due to incomplete ablation of Piezo2 from inducible Cre activity[15]. We also monitored basal respiratory activities in *Phox2bCre;Piezo2^{cKO}* mice and, as expected, these mice showed increased tidal volume and normal breathing frequency compared to wild-type littermates (Extended Data Fig. 8a, b).

To further characterize Piezo2 as the airway mechanotransducer, we assayed Hering–Breuer mechanoreflex responses in both *Phox2bCre;Piezo2^{cKO}* and *AdvillinCreER^{T2};Piezo2^{cKO}* mice. Although wild-type littermate mice showed a clear halt of respiration as their lungs were inflated, both *Phox2bCre;Piezo2^{cKO}* and *AdvillinCreER^{T2};Piezo2^{cKO}* mice continued their normal respiration, indicating that this mechanoreflex was impaired in both strains of Piezo2-deficient mice (Fig. 5c, d, Extended Data Fig. 8c). We also performed a control experiment to test the respiratory reflex to a non-mechanical stimulus in Piezo2-deficient mice. Intravenous injection of the C-fibre activator phenylbiguanide (PBG) resulted in acute apnoea in both wild-type and *AdvillinCreER^{T2};Piezo2^{cKO}* mice (Extended Data Fig. 8d, e), indicating that the chemoreflex response is normal in Piezo2-deficient mice. We also considered the possible involvement of Piezo2-mediated proprioception in respiratory control, as proprioceptors might provide feedback on respiratory muscle activities[34]. *PvalbCre;Piezo2^{cKO}* mice, in which proprioception is impaired[17], showed an intact Hering–Breuer reflex and normal breathing parameters, suggesting that Piezo2 in proprioceptive neurons is not essential for the airway mechanoreflex and basal respiration (Extended Data Figs 7e, f, 8f–h). Our data suggest that Piezo2 expressed in the nodose ganglia is the major mechanotransducer required for the Hering–Breuer reflex and respiratory volume control in adult mice.

Discussion

Our analyses, via selective activation of Piezo2^{+} sensory neurons and conditional ablation of Piezo2 channels, have uncovered roles for airway mechanotransduction in respiratory physiology. Piezo2 in nodose sensory neurons is a stretch sensor that is required for lung volume regulation and the Hering–Breuer reflex in adult mice, whereas Piezo2 in sensory neurons of neural crest origin is required for proper lung expansion and the onset of efficient respiration in newborn mice (Extended Data Fig. 9). Our mouse genetics data demonstrate that Piezo2 is a versatile mechanotransducer, functioning as a sensor of lung inflation in addition to touch and proprioception[15,17]. Recently, humans carrying compound inactivating variants of *PIEZO2* were reported to have selective loss of discriminative touch perception and profoundly decreased proprioception; these individuals also exhibited shallow breathing during infancy[35,36]. Thus, the general role of Piezo2 in somatosensory mechanotransduction is conserved between mice and humans.

Beyond the regulation of normal respiration, airway mechanotransduction might contribute to respiratory diseases. We previously reported that a subtype of distal arthrogryposis type 5 (DA5) is caused by autosomal dominant mutations of *PIEZO2* with slower inactivation kinetics than the wild-type channel[37]. Most patients with DA5 suffer from joint contractures and develop restrictive lung diseases[37,38]. Our data raise the possibility that overactivation of PIEZO2^{+} vagal neurons might overtly increase lung stretch responses in these patients and lead to respiratory complications. Moreover, compromised mechanotransduction in the respiratory system (possibly via PIEZO2) could play a more substantial role in the clinic. For example, an attenuated Hering–Breuer reflex is reported in patients with chronic obstructive pulmonary disease (COPD)[39]. Sleep apnoea in adults and/or sudden infant death syndrome has also been suggested to be associated with dysfunctions in sensory neurons innervating the upper airway, including the oral and nasal cavities and larynx[3,40–42].

As shown in the respiratory system, mechanical forces serve as cues to trigger subsequent biological responses in many visceral organs, but the mechanisms or physiological importance of mechanotransduction in other visceral organs has not been fully elucidated[14]. Our study suggests that genetic manipulations of *Piezo2* in mice could be used to explore the role of mechanotransduction in other biological processes within the viscera, such as heart rate control, satiety, and bladder function[35,36,43–45].

Online Content Methods, along with any additional Extended Data display items and Source Data, are available in the online version of the paper; references unique to these sections appear only in the online paper.

Received 15 February; accepted 16 November 2016.
Published online 21 December 2016.

1. Rhoades, R. A. & Bell, D. R. *Medical Physiology: Principles for Clinical Medicine* 3rd edn, 328 (Lippincott Williams & Wilkins, 2009).
2. Schelegle, E. S. & Green, J. F. An overview of the anatomy and physiology of slowly adapting pulmonary stretch receptors. *Respir. Physiol.* **125,** 17–31 (2001).
3. Lee, L. Y. & Yu, J. Sensory nerves in lung and airways. *Compr. Physiol.* **4,** 287–324 (2014).
4. Zhang, J. W., Walker, J. F., Guardiola, J. & Yu, J. Pulmonary sensory and reflex responses in the mouse. *J. Appl. Physiol.* **101,** 986–992 (2006).
5. Carr, M. J. & Undem, B. J. Bronchopulmonary afferent nerves. *Respirology* **8,** 291–301 (2003).
6. Kaczyńska, K. & Szereda-Przestaszewska, M. Nodose ganglia-modulatory effects on respiration. *Physiol. Res.* **62,** 227–235 (2013).
7. Belvisi, M. G. Overview of the innervation of the lung. *Curr. Opin. Pharmacol.* **2,** 211–215 (2002).
8. Alexandrova, N. P., Donina, Z. A. & Danilova, G. A. Effect of central hypervolemia on respiratory function. *J. Physiol. Pharmacol.* **58** (Suppl. 5), 9–15 (2007).
9. Chang, R. B., Strochlic, D. E., Williams, E. K., Umans, B. D. & Liberles, S. D. Vagal sensory neuron subtypes that differentially control breathing. *Cell* **161,** 622–633 (2015).
10. Turgeon, B. & Meloche, S. Interpreting neonatal lethal phenotypes in mouse mutants: insights into gene function and human diseases. *Physiol. Rev.* **89,** 1–26 (2009).
11. Rabbette, P. S. & Stocks, J. Influence of volume dependency and timing of airway occlusions on the Hering-Breuer reflex in infants. *J. Appl. Physiol.* **85,** 2033–2039 (1998).
12. Wong, K. A. *et al.* Pulmonary vagal innervation is required to establish adequate alveolar ventilation in the newborn lamb. *J. Appl. Physiol.* **85,** 849–859 (1998).
13. Hasan, S. U., Lalani, S. & Remmers, J. E. Significance of vagal innervation in perinatal breathing and gas exchange. *Respir. Physiol.* **119,** 133–141 (2000).

14. Ranade, S. S., Syeda, R. & Patapoutian, A. Mechanically activated ion channels. *Neuron* **87,** 1162–1179 (2015).
15. Ranade, S. S. *et al.* Piezo2 is the major transducer of mechanical forces for touch sensation in mice. *Nature* **516,** 121–125 (2014).
16. Coste, B. *et al.* Piezo1 and Piezo2 are essential components of distinct mechanically activated cation channels. *Science* **330,** 55–60 (2010).
17. Woo, S. H. *et al.* Piezo2 is the principal mechanotransduction channel for proprioception. *Nat. Neurosci.* **18,** 1756–1762 (2015).
18. Schrenk-Siemens, K. *et al.* PIEZO2 is required for mechanotransduction in human stem cell-derived touch receptors. *Nat. Neurosci.* **18,** 10–16 (2015).
19. Dubin, A. E. *et al.* Inflammatory signals enhance piezo2-mediated mechanosensitive currents. *Cell Reports* **2,** 511–517 (2012).
20. Pei, L. *et al.* Thyroid hormone receptor repression is linked to type I pneumocyte-associated respiratory distress syndrome. *Nat. Med.* **17,** 1466–1472 (2011).
21. Woo, S. H. *et al.* Piezo2 is required for Merkel-cell mechanotransduction. *Nature* **509,** 622–626 (2014).
22. Pan, J., Copland, I., Post, M., Yeger, H. & Cutz, E. Mechanical stretch-induced serotonin release from pulmonary neuroendocrine cells: implications for lung development. *Am. J. Physiol. Lung Cell. Mol. Physiol.* **290,** L185–L193 (2006).
23. Cutz, E., Pan, J., Yeger, H., Domnik, N. J. & Fisher, J. T. Recent advances and contraversies on the role of pulmonary neuroepithelial bodies as airway sensors. *Semin. Cell Dev. Biol.* **24,** 40–50 (2013).
24. Smith, J. C., Abdala, A. P., Rybak, I. A. & Paton, J. F. Structural and functional architecture of respiratory networks in the mammalian brainstem. *Phil. Trans. R. Soc. Lond. B* **364,** 2577–2587 (2009).
25. Koni, P. A. *et al.* Conditional vascular cell adhesion molecule 1 deletion in mice: impaired lymphocyte migration to bone marrow. *J. Exp. Med.* **193,** 741–754 (2001).
26. Danielian, P. S., Muccino, D., Rowitch, D. H., Michael, S. K. & McMahon, A. P. Modification of gene activity in mouse embryos in utero by a tamoxifen-inducible form of Cre recombinase. *Curr. Biol.* **8,** 1323–1326 (1998).
27. Scott, M. M., Williams, K. W., Rossi, J., Lee, C. E. & Elmquist, J. K. Leptin receptor expression in hindbrain Glp-1 neurons regulates food intake and energy balance in mice. *J. Clin. Invest.* **121,** 2413–2421 (2011).
28. Nassenstein, C. *et al.* Phenotypic distinctions between neural crest and placodal derived vagal C-fibres in mouse lungs. *J. Physiol. (Lond.)* **588,** 4769–4783 (2010).
29. Chai, Y. *et al.* Fate of the mammalian cranial neural crest during tooth and mandibular morphogenesis. *Development* **127,** 1671–1679 (2000).
30. Li, B. Y., Glazebrook, P., Kunze, D. L. & Schild, J. H. KCa1.1 channel contributes to cell excitability in unmyelinated but not myelinated rat vagal afferents. *Am. J. Physiol. Cell Physiol.* **300,** C1393–C1403 (2011).
31. Ruan, H. Z. & Burnstock, G. Localisation of P2Y1 and P2Y4 receptors in dorsal root, nodose and trigeminal ganglia of the rat. *Histochem. Cell Biol.* **120,** 415–426 (2003).
32. Lee, K. Z. *et al.* Hypoglossal neuropathology and respiratory activity in pompe mice. *Front. Physiol.* **2,** 31 (2011).
33. McGovern, A. E. *et al.* Evidence for multiple sensory circuits in the brain arising from the respiratory system: an anterograde viral tract tracing study in rodents. *Brain Struct. Funct.* **220,** 3683–3699 (2015).
34. Parkes, M. J. Breath-holding and its breakpoint. *Exp. Physiol.* **91,** 1–15 (2006).
35. Chesler, A. T. *et al.* The role of PIEZO2 in human mechanosensation. *N. Engl. J. Med.* **375,** 1355–1364 (2016).
36. Delle Vedove, A. *et al.* Biallelic loss of proprioception-related PIEZO2 causes muscular atrophy with perinatal respiratory distress, arthrogryposis, and scoliosis. *Am. J. Hum. Genet.* **99,** 1206–1216 (2016).
37. Coste, B. *et al.* Gain-of-function mutations in the mechanically activated ion channel PIEZO2 cause a subtype of distal arthrogryposis. *Proc. Natl Acad. Sci. USA* **110,** 4667–4672 (2013).
38. Okubo, M. *et al.* A family of distal arthrogryposis type 5 due to a novel PIEZO2 mutation. *Am. J. Med. Genet. A.* **167A,** 1100–1106 (2015).
39. Tryfon, S., Kontakiotis, T., Mavrofridis, E. & Patakas, D. Hering–Breuer reflex in normal adults and in patients with chronic obstructive pulmonary disease and interstitial fibrosis. *Respiration* **68,** 140–144 (2001).
40. Nishino, T. Physiological and pathophysiological implications of upper airway reflexes in humans. *Jpn J. Physiol.* **50,** 3–14 (2000).
41. Thach, B. T. The role of respiratory control disorders in SIDS. *Respir. Physiol. Neurobiol.* **149,** 343–353 (2005).
42. Ramirez, J. M. *et al.* Central and peripheral factors contributing to obstructive sleep apneas. *Respir. Physiol. Neurobiol.* **189,** 344–353 (2013).
43. Fox, E. A. *et al.* Neurotrophin-4 deficient mice have a loss of vagal intraganglionic mechanoreceptors from the small intestine and a disruption of short-term satiety. *J. Neurosci.* **21,** 8602–8615 (2001).
44. Lu, Y. *et al.* The ion channel ASIC2 is required for baroreceptor and autonomic control of the circulation. *Neuron* **64,** 885–897 (2009).
45. Sun, B., Li, Q., Dong, L. & Rong, W. Ion channel and receptor mechanisms of bladder afferent nerve sensitivity. *Auton. Neurosci.* **153,** 26–32 (2010).

Supplementary Information is available in the online version of the paper.

Acknowledgements We thank D. Trajkovic for assistance with histology; M. Wood for assistance with electron microscopy; J. Yu for suggesting that we test the Hering–Breuer reflex; S. M. Cahalan, M. Petrus, J. Mathur, K. Marshall, S. Lee, T. Kawamura, J. Chen and P. Paolo Sanna for technical assistance; and M. Krasnow for discussions. This research was supported by NIH grants R01DE022358 to A.P. and R01HL132255, and a Giovanni Armenise-Harvard Foundation Grant to S.D.L. A.P. is an investigator of the Howard Hughes Medical Institute.

Author Contributions A.G. characterized embryonic lungs in the laboratory of M. Krasnow. Z.Q. performed the initial characterization of *Piezo2*$^{-/-}$ mice. A.G.F. performed plethysmograph recordings and behavioural experiments to confirm Piezo2 knockdown. S.S.R. generated *Piezo2*$^{fl/fl}$ and *Piezo2*$^{+/-}$ mice. R.B.C. performed optogenetic experiments, whole vagus nerve electrophysiology recordings, and transducer-based Hering–Breuer reflex assessment in the S.D.L. laboratory. K.N. and S.-H.W. contributed equally to all other experiments. K.N., S.-H.W. and A.P. wrote the manuscript.

Author Information Reprints and permissions information is available at www.nature.com/reprints. The authors declare no competing financial interests. Readers are welcome to comment on the online version of the paper. Correspondence and requests for materials should be addressed to A.P. (ardem@scripps.edu) or S.D.L (Stephen_Liberles@hms.harvard.edu).

Reviewer Information *Nature* thanks C. Goridis and the other anonymous reviewer(s) for their contribution to the peer review of this work.

METHODS

All animal procedures were approved by the Institutional Animal Care and Use Committees of The Scripps Research Institute and Harvard Medical School.

Mouse lines. *Piezo2*$^{-/-}$ mice were generated by breeding *Piezo2*$^{fl/fl}$ and *EIIaCre* mice[21] (The Jackson Laboratory, stock# 3724). The *Piezo2*^{GFP}*-IRES-Cre* (*Piezo2*^{GFP}) mouse line has been previously described[21]. *Tie2Cre;Piezo2*$^{cKO(fl/-)}$, *Phox2bCre;Piezo2* $^{cKO(fl/-)}$, *Wnt1Cre;Piezo2* $^{cKO(fl/-)}$, *PvalbCre;Piezo2* $^{cKO(fl/-)}$ and *AdvillinCreER*^{T2}*;Piezo2*$^{fl/-}$ (before Tam induction) mice were generated by breeding *Tie2Cre* (stock# 4128), *Phox2bCre* (stock# 16223), *Wnt1Cre* (stock# 3829), *PvalbCre* (stock# 8069) *or AdvillinCreER*^{T2} lines[15] with *Piezo2*$^{fl/fl}$ and *Piezo2*$^{+/-}$ mice. Each of these Cre mouse lines was also crossed to *Ai9* reporters (stock# 7909). *Piezo2*^{GFP}*;lox-ChR2* mice were generated by breeding *Piezo2*^{GFP} mice with *lox-ChR2* mice (stock# 12569).

Histology. *Haematoxylin and eosin staining.* Lungs were removed from either embryonic day (E)18.5 mouse embryos or newborn mice and processed for paraffin embedding. Paraffin sections were deparaffinized before haematoxylin and eosin staining.

Immunofluorescence. For Extended Data Figs 2, 3, lungs, trigeminal ganglion, diaphragm and intercostal muscles were removed from newborn mouse pups. The jugular–nodose complex and brainstem were removed from both newborn mouse pups and adult mice. Tracheal parasympathetic ganglia were removed from adult mice. DRG and sympathetic ganglia were isolated from the upper thoracic region (Th1–3) of adult mice. Spinal cord from the lumbar region was isolated from postnatal mice. All tissues were briefly fixed in 4% paraformaldehyde (PFA)/phosphate buffered saline (PBS) and then incubated in 30% sucrose/PBS overnight at 4 °C. Fixed tissues were cryo-embedded in OCT compound (Sakura) and cryo-sectioned for immunofluorescence as previously described[21].

Analysis of lung branching, vessel pattern and alveolar epithelial differentiation by whole-mount immunostaining. Lungs were removed from E16.5 and E18.5 mouse embryos and fixed in 80% methanol/20% dimethylsulfoxide (DMSO) overnight at 4 °C. Whole lobes from E16.5 and E18.5 mice were stained for αSMA to visualize conducting airways, arteries and veins. Whole lobes from E18.5 mice were stained for E-cadherin, Muc1, T1α, and SpC to assess distal epithelial morphology and to visualize alveolar progenitors and nascent type I and II pneumocytes. Whole-mount immunostaining was performed as previously described[46] with the following modifications: lobes were incubated with primary antibodies diluted in blocking solution (PBS with 5% donkey serum, 3% bovine serum albumin (BSA) and 0.5% Triton-X-100) for three nights at 4 °C and with secondary antibodies conjugated to Alexa fluorophores (488, 568, 647) for two nights at 4 °C. Stained specimens were dehydrated in methanol and cleared in benzyl alcohol:benzyl benzoate (1:2). Samples were imaged on chambered coverslips with an inverted laser scanning confocal microscope (Zeiss LSM780).

Antibodies. The following antibodies were used: GFP (1:500, Life Technologies, A10262 or A11122); Nefh (1:1,000, Aves laboratory, NFH or 1:1,000, Abcam, ab8135); CGRP (1:500, Abcam, ab43873); NeuN (1:500, Millipore, MAB377); PECAM1 (1:100, Abcam, ab28364); PV (1:500, Swant, PV 2); α-bungarotoxin (1:500, Life Technologies, B13423); advillin (1:500, Abcam, ab72210); Tuj1 (1:500, Covance, MMS-435P-250); αSMA–Cy3 (1:200, Sigma, C6198); E-cadherin (1:500, Life Technologies, 13-1900); MUC-1 (1:500, Fisher Scientific, HM1630P0); T1α (1:50, DSHB, 8.1.1); proSP-C (1:300, Millipore, AB3786); ChAT (1:300, Millipore, AB143); Piezo2 (1:1,000)[21]; IB4-Alexa Fluor568 conjugate (1:200, Life Technologies, I21412).

Pulse oximetry. Newborn mouse pups were subjected to pulse oximetry and heart rate recordings (MouseSTAT, Kent Scientific Corporation). The heads of newborn mice were placed in a ring-shaped oxygen sensor and the mice were allowed to acclimatize for 1 min, and then O_2 saturation levels (% SpO_2) and heart rates were recorded every 15 s for 5 min. O_2 saturation levels associated with heart rates greater than 200 b.p.m. were used for data analyses for reliability and accuracy.

Whole-body plethysmography. Freely behaving newborn and anaesthetized adult mice were subjected to whole-body plethysmography (Buxco system, DSI)[47]. Data were analysed with FinePointe software (Buxco system, DSI). For data from newborn mice, respiratory frequency was manually analysed by counting the number of inspiratory peaks with peak flow more than 0.3 ml/s and these were distinguished from background levels monitored when the chamber was empty. Values for air flow of newborn mice are possibly imprecise owing to technical limitations of monitoring respiration in newborn mice, while measurements of respiratory frequencies are precise[48]. Adult (10–14 weeks old) mice were anaesthetized with 1% isoflurane in 0.4 l/min oxygen supply during recording and data were collected for 10 min after a 15 min acclimation period in the recording chamber.

Wet-to-dry weight ratio. E18.5 embryos were delivered by caesarean section and were induced to breathe. Lungs were removed 6 h after delivery. After removing excess liquid by blotting, lung samples were weighed (wet weight). Next, the samples were dried overnight at 80 °C, and re-weighed the next day (dry weight). Water content of lungs was determined by the difference between the wet and dry weights[49].

Electron microscopy. Lungs from newborn mice were placed in ice cold fixative consisting of 1% PFA + 3% glutaraldehyde in 0.1 M cacodylate buffer +5 mM $CaCl_2$ pH 7.3 overnight. Following a wash in cacodylate buffer, the tissues were further fixed in 1% OsO_4 with 0.75% potassium ferricyanide in 0.1 M cacodylate buffer for 2 h, again washed in cacodylate buffer and then dehydrated in a graded ethanol series followed by transitioning in propylene oxide. The lung tissue pieces were embedded in Embed 812/Araldite (Electron Microscopy Sciences). Thick sections (2 μm) were cut, mounted on glass slides and stained in toluidine blue for general assessment of the tissues in the light microscope. Subsequently, 70 nm thin sections were cut, mounted on copper slot grids coated with parlodion and stained with uranyl acetate and lead citrate for examination on a Philips CM100 electron microscope (FEI) at 80 kV. Images were documented using a Megaview III ccd camera (Olympus Soft Imaging Solutions GmbH).

Adeno-associated virus (AAV) infections of the J–N complex. AAV infection of the J–N complex was performed as previously described[9]. Briefly, after the left J–N complex of adult mice was surgically exposed under anaesthesia by making an incision along the ventral surface of the neck and blunt dissection, a micropipette containing *AAV-flex-tdTomato* (Penn Vector Core, AV-9-ALL867, titre 1.3×10^{13} genome copies per ml) was inserted into the J–N complex. Virus solution was injected (140 nl) using a Nanoject II. Animals recovered from surgery and were killed 4–8 weeks later for tissue removal.

Retrograde tracing of neurons innervating the lung. Surgery was carried out on 8–10-week-old *Piezo2*^{GFP} mice. After mice were anaesthetized using isoflurane, the trachea was exposed by a midline cervical incision. 1 μl of the fluorescent tracer (1% DiO in *N,N*-dimethylformamide (DMF)) was injected into the tracheal lumen between two cartilage rings close to the bronchus using a microsyringe[50,51]. The animals were sutured and were allowed to recover for 7 days for sufficient labelling of cell bodies. On the eighth day after surgery, all animals were killed and ganglia were removed. The J–N complex, upper thoracic (Th1–3) DRG, and lumbar DRG were collected from each animal for cryo-sectioning and immunofluorescence. The lumbar DRG served as a control: animals with DiO labelling in their lumbar DRG were removed from the experimental cohort as this indicated leakage of DiO during injection.

Quantitative real-time polymerase chain reaction (qRT–PCR). For *Tie2Cre;Piezo2*^{cKO} and control mice, lungs were removed from adult mice ($n = 4$) and were processed into a single-cell suspension. Cells were then stained with PE-conjugated CD31 antibody (BD Pharmingen) for 30 min to 1 h on ice and were subjected to fluorescence-activated cell sorting (FACS). $DAPI^+$ cells were excluded, and $DAPI^-$ $CD31^+$ and $DAPI^-$ $CD31^-$ cells were sorted into separate tubes containing TRIzol. Total RNA was isolated for qRT–PCR. For *Wnt1Cre;Piezo2*^{cKO} and control pups, DRG were removed from newborn pups ($n = 5$) and placed into TRIzol. Total RNA was isolated and subjected to qRT–PCR as previously described[4].

***In situ* hybridization.** The jugular–nodose complex was isolated from adult mice and fixed in 4% PFA/PBS for 4 h on ice. They were then incubated in 30% sucrose/PBS overnight at 4 °C. On the next day, fixed tissues were cryo-embedded in OCT compound and cryo-sectioned at 8 μm. Sections were subjected to *in situ* hybridization according to the manufacturer's protocol (Advanced Cell Diagnostics).

Optogenetic stimulations and analyses. Optogenetic stimulation of the vagus nerve was performed as previously described[9]. Mice were deeply anaesthetized (isoflurane, 1.5–2%, Abbott Laboratory), freely breathing, and maintained at normal body temperature. Briefly, in order to measure the conduction velocity of vagal sensory neurons, a short light pulse (0.8 ms) was delivered via an optic fibre positioned on the left vagus nerve trunk 1 mm beneath the recording electrodes and coupled to a laser light source (473 nm, 150 mW, Ultralaser). Light-induced compound action potentials were recorded by whole-nerve electrophysiology (50 kHz sampling rate), amplified (CP511, Grass), and acquired with a data acquisition system (MP150, Biopac). Fibre conduction velocity was determined by varying the distance between the optic fibre and recording electrode (travel distance); the resulting time lags in peak maxima (Δt) were plotted as a function of travel distance, revealing characteristic A and C fibre types. The total currents carried by A or C fibres were calculated by integrating the corresponding peak area in the compound action potential. The A–C ratio reported here may underrepresent fold enrichment as the A and C peaks were not completely separated in most recordings. In order to investigate the effect of $Piezo2^+$ vagal sensory neuron activation on respiration, light stimulations (5 ms pulses at 50 Hz, 75–125 mW/mm^2 intensity) were delivered to the base of the left nodose ganglion. Respiration rate was measured using an amplifier-coupled pressure transducer (Cwe) cannulated into the trachea. A breath was scored if the lung volume increased to at least 10%

of mean tidal volume. Total lung volume was calculated by integrating lung volume across 10-s periods during baseline and stimulation with or without light. High volume state was defined as greater than mean volume during tidal breathing.

Tamoxifen treatment. Tamoxifen (Sigma) dissolved in corn oil was injected as previously described[15]. Briefly, in adult *AdvillinCreER^{T2};Piezo2$^{fl/-}$* (test) and *Piezo2$^{fl/+}$* (control) mice, tamoxifen was injected at 150 mg/kg (body weight) for 5 consecutive days. The mice were allowed to recover for 1 week, and they were subjected to a static force von Frey test to confirm Piezo2 knockdown[15]. Mice with efficient Piezo2 knockdown (mice displaying reduced sensitivity to low threshold mechanical stimuli) were subjected to plethysmography recordings, the Hering–Breuer reflex test or whole vagus nerve electrophysiology recording the following week. *AdvillinCreER^{T2};Piezo2^{cKO}* mice refer to *AdvillinCreER^{T2};Piezo2$^{fl/-\,(+\,Tam)}$*, and WT mice refer to *Piezo2$^{fl/+\,(+\,Tam)}$*.

Whole vagus nerve electrophysiology recording. Whole vagus nerve electrophysiology recording was performed as previously described[9]. Briefly, in deeply anaesthetized mice (isoflurane, 1.5–2%, Abbott Laboratory), the left vagus nerve was cervically transected, and the peripheral transected end was desheathed and placed onto a pair of platinum-iridium electrodes. In the case of nerve recording with artificial airway inflation, air was introduced into the airway at a flow rate of 200, 400, 600 or 800 cc/min via a tracheal cannula (PE-50, Braintree Scientific), while the mice were kept anaesthetized with 1.5–2% isoflurane gas supplied through another tracheal cannula. Multiunit neural activity was amplified (CP511, Grass Technologies), digitized (MP150, Biopac), recorded with AcqKnowledge data acquisition program (Biopac), and integrated with a time constant of 1 s. Lung-inflation-induced responses were calculated by subtracting baseline neural activity from activity recorded during stimulus. The response to serotonin (10 mM, 400 µl, intraperitoneal injection) over a 100-s period after administration was used for normalization.

The Hering–Breuer reflex test. *Phox2bCre;Piezo2^{cKO}* and wild-type littermate mice (10–14 weeks old) were deeply anesthetized (isoflurane, 1.5–2%, Abbott Laboratory), freely breathing, and maintained at normal body temperature. Airway pressure was measured using an amplifier-coupled pressure transducer (Cwe) cannulated into the trachea and recorded with a M150 data acquisition system (Biopac). A breath was scored if lung volume was increased to at least 10% of mean tidal volume. Air was introduced into the airway at flow rate of 200, 400, 600 or 800 cc/min via a tracheal cannula (PE-50, Braintree Scientific). *AdvillinCreER^{T2};Piezo2^{cKO}*, *PvalbCre;Piezo2^{cKO}* mice and their wild-type littermates (10–14 weeks old) were anaesthetized with 200 mg/kg (body weight) ketamine HCl (Henry Schein) injected intraperitoneally. The depth of anaesthesia was assessed in terms of movement reactions to tactile stimulation. The trachea was exposed by a midline cervical incision. The trachea was then cut horizontally between two cartilage rings, and an 18 G needle attached to a three-way stopcock was inserted into the trachea lumen. One end of the three-way stopcock was attached to a syringe (through which air was injected), and the other end could be 'open' or 'closed'. Shortly after the needle was placed in the trachea, mice were left to vent freely through the open end to obtain a baseline breathing pattern. After the baseline was obtained, the open end was switched to the closed position so that air from outside was blocked, and then 0.3 ml air was injected through the syringe into the trachea[4]. After air was injected, the three-way stopcock was kept closed for 8–10 s, and then was opened so that mice could resume their autonomous breathing. Respiratory activities throughout the experiment were videotaped and were quantified by movement of the abdomen. The number of respiratory activities observed between 2 and 6 s after air injection was normalized to the baseline and was compared between Piezo2-deficient and wild-type mice.

Phenylbiguanide (PBG) induced C-fibre-mediated pulmonary reflex. *AdvillinCreER^{T2};Piezo2^{cKO}* and wild-type mice (10–14 weeks old) were anaesthetized with 1.5 g/kg (body weight) urethane (SPEX CertiPrep) injected intraperitoneally. The depth of anaesthesia was assessed in terms of movement reactions to tactile stimulation. The experiment was performed as previously described[4]. Briefly, PBG (Sigma-Aldrich, 100 µg/ml, 20 µl) was administrated intravenously after the left femoral vein was cannulated with polyethylene tubing. Respiratory pattern was monitored by an air flow sensor (Buxco system, DSI).

Statistics. All data analysed by statistical analyses are detailed in the figure legends. All statistical analyses were performed with GraphPad Prism6. When unpaired Student's *t*-test was applied, similarity of variance between groups was confirmed by *F* test. Data from qPCR experiments of isolated DRG or endothelial cells were analysed by unpaired Welch's *t*-test. Oxygen saturation levels in blood were analysed by Mann–Whitney test. Wet to dry lung ratio data were analysed by unpaired Student's *t*-test. Weight of lung or liver was analysed by Kruskal–Wallis nonparametric test. Weight of heart was analysed by one-way ANOVA. Respiratory parameters were analysed by Student's or Welch's *t*-test. Data of whole vagus nerve electrophysiology recording and Hering-Breuer reflex with air flow of multiple steps were analysed by repeated measures two-way ANOVA with Sidak's post-hoc. All statistical analyses were two-sided.

Sample size choice. The specific number of independent experiments or animal numbers used for all experiments is outlined in the corresponding figures or their legends. For qRT–PCR analysis, sample sizes were chosen on the basis of our previous studies, in which we performed at least three separate experiments per sample to ensure statistical significance. For oxygen saturation levels in blood, data were obtained from between 4 and 40 animals per genotype. All respiratory parameters or whole vagus nerve electrophysiology recording data represent results from 2–4 independent rounds of testing with multiple mice of both genotypes per cohort. All mice tested were littermate controls. Both male and female mice were used for all experiments. *AdvillinCreER^{T2};Piezo2^{cKO}* mice were subjected to static force von Frey test based on our previous studies to confirm Piezo2 knockdown before experiments. All experimental procedures were performed in a blinded manner. No randomization was applied. No statistical method was used to predetermine sample size.

Data availability. The datasets generated during and/or analysed during the current study are available from the corresponding author on reasonable request.

46. Metzger, R. J., Klein, O. D., Martin, G. R. & Krasnow, M. A. The branching programme of mouse lung development. *Nature* **453,** 745–750 (2008).
47. Massey, C. A. *et al.* Isoflurane abolishes spontaneous firing of serotonin neurons and masks their pH/CO_2 chemosensitivity. *J. Neurophysiol.* **113,** 2879–2888 (2015).
48. Ramanantsoa, N. *et al.* Ventilatory response to hyperoxia in newborn mice heterozygous for the transcription factor Phox2b. *Am. J. Physiol. Regul. Integr. Comp. Physiol.* **290,** R1691–R1696 (2006).
49. Barker, P. M. & Gatzy, J. T. Effect of gas composition on liquid secretion by explants of distal lung of fetal rat in submersion culture. *Am. J. Physiol.* **265,** L512–L517 (1993).
50. Kwong, K. *et al.* Voltage-gated sodium channels in nociceptive versus non-nociceptive nodose vagal sensory neurons innervating guinea pig lungs. *J. Physiol. (Lond.)* **586,** 1321–1336 (2008).
51. Dinh, Q. T. *et al.* Substance P expression in TRPV1 and trkA-positive dorsal root ganglion neurons innervating the mouse lung. *Respir. Physiol. Neurobiol.* **144,** 15–24 (2004).
52. Chamberlin, N. L. Functional organization of the parabrachial complex and intertrigeminal region in the control of breathing. *Respir. Physiol. Neurobiol.* **143,** 115–125 (2004).
53. Driessen, A. K., Farrell, M. J., Mazzone, S. B. & McGovern, A. E. The role of the paratrigeminal nucleus in vagal afferent evoked respiratory reflexes: a neuroanatomical and functional study in guinea pigs. *Front. Physiol.* **6,** 378 (2015).
54. Bonham, A. C. & McCrimmon, D. R. Neurones in a discrete region of the nucleus tractus solitarius are required for the Breuer-Hering reflex in rat. *J. Physiol. (Lond.)* **427,** 261–280 (1990).
55. Mortola, J. P. *Respiratory Physiology of Newborn Mammals* 24–37 (Johns Hopkins Univ. Press, 2001).
56. Woo, S. H., Lumpkin, E. A. & Patapoutian, A. Merkel cells and neurons keep in touch. *Trends Cell Biol.* **25,** 74–81 (2015).
57. Vijayaraghavan, R. *et al.* Computer assisted recognition and quantitation of the effects of airborne chemicals acting at different areas of the respiratory tract in mice. *Arch. Toxicol.* **68,** 490–499 (1994).
58. Hamelmann, E. *et al.* Noninvasive measurement of airway responsiveness in allergic mice using barometric plethysmography. *Am. J. Respir. Crit. Care Med.* **156,** 766–775 (1997).

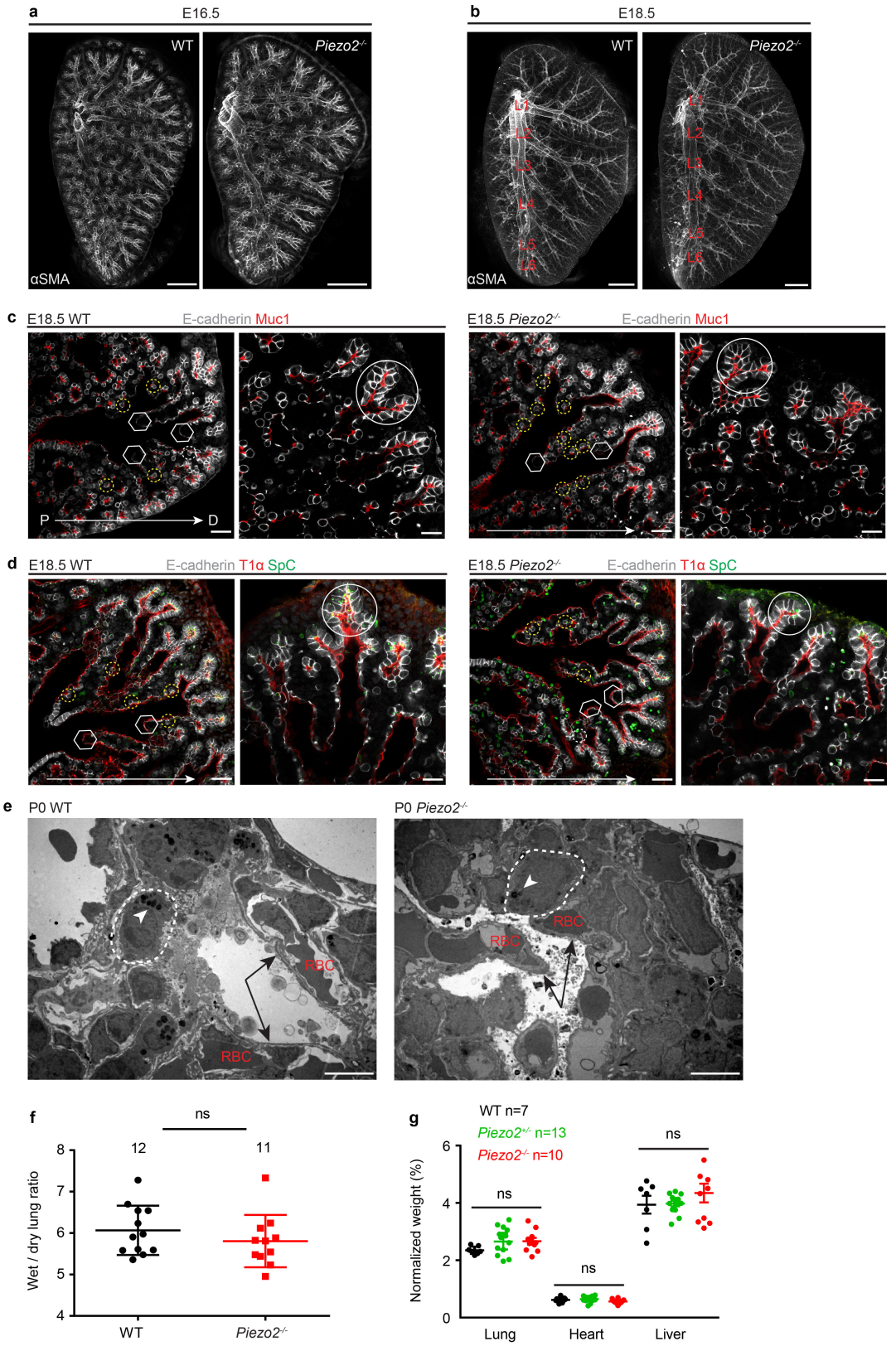

Extended Data Figure 1 | See next page for caption.

Extended Data Figure 1 | Characterization of lung development in *Piezo2*$^{-/-}$ mice. a, **b**, Whole-mount staining for αSMA in the left lobe of lungs from E16.5 (**a**) and E18.5 (**b**) wild-type and *Piezo2*$^{-/-}$ mice. L1–L6, lateral branches of the left lobe. E16.5: wild-type $n = 4$, *Piezo2*$^{-/-}$ $n = 3$; E18.5: wild-type $n = 4$, *Piezo2*$^{-/-}$ $n = 5$. A normal conducting airway and vessel pattern was observed in *Piezo2*$^{-/-}$ lungs at late embryonic stages. **c**, **d**, Whole-mount immunostaining for E-cadherin and Muc-1 (**c**) or E-cadherin, T1α, and SpC (**d**) in left lobes from E18.5 wild-type and *Piezo2*$^{-/-}$ mice. Arrows indicate proximal (P) to distal (D) direction. Left panels, lower magnification; right panels, higher magnification of the distal region. Solid circles in right panels indicate alveolar progenitors in the distal region. Solid hexagons in left panels indicate nascent type I pneumocytes. Yellow dashed circles in left panels indicate nascent type II pneumocytes. A normal epithelial morphology and no defects in alveolar epithelial patterning and differentiation were observed *Piezo2*$^{-/-}$ lungs. **e**, Representative ultrastructures of wild-type and *Piezo2*$^{-/-}$ newborn lungs. Black arrows mark type I pneumocyte extensions. White dotted circles mark type II pneumocytes. White arrowheads within white dotted circles mark lamellar bodies. RBC, red blood cells. Samples from four mice per genotype were analysed. Normal morphology and similar abundances of type I and II pneumocytes, endothelial cells, red blood cells and surfactant proteins were observed in *Piezo2*$^{-/-}$ lungs compared to wild-type lungs. **f**, Wet-to-dry lung ratio 6 h after delivery at E18.5 to assess clearance of fetal pulmonary fluid. NS, statistically not significant. Unpaired Student's *t*-test. Bars represent mean ± s.d. **g**, Per cent weight of postnatal day (P)0 lung, heart, and liver normalized to whole body weight. Bars represent mean ± s.e.m. NS, statistically not significant. Kruskal–Wallis nonparametric test (lung and liver) or one-way ANOVA (heart). Scale bars, 500 μm (**a**, **b**); 33 μm (**c**, **d**, left); 22 μm (**c**, **d**, right); 5 μm (**e**).

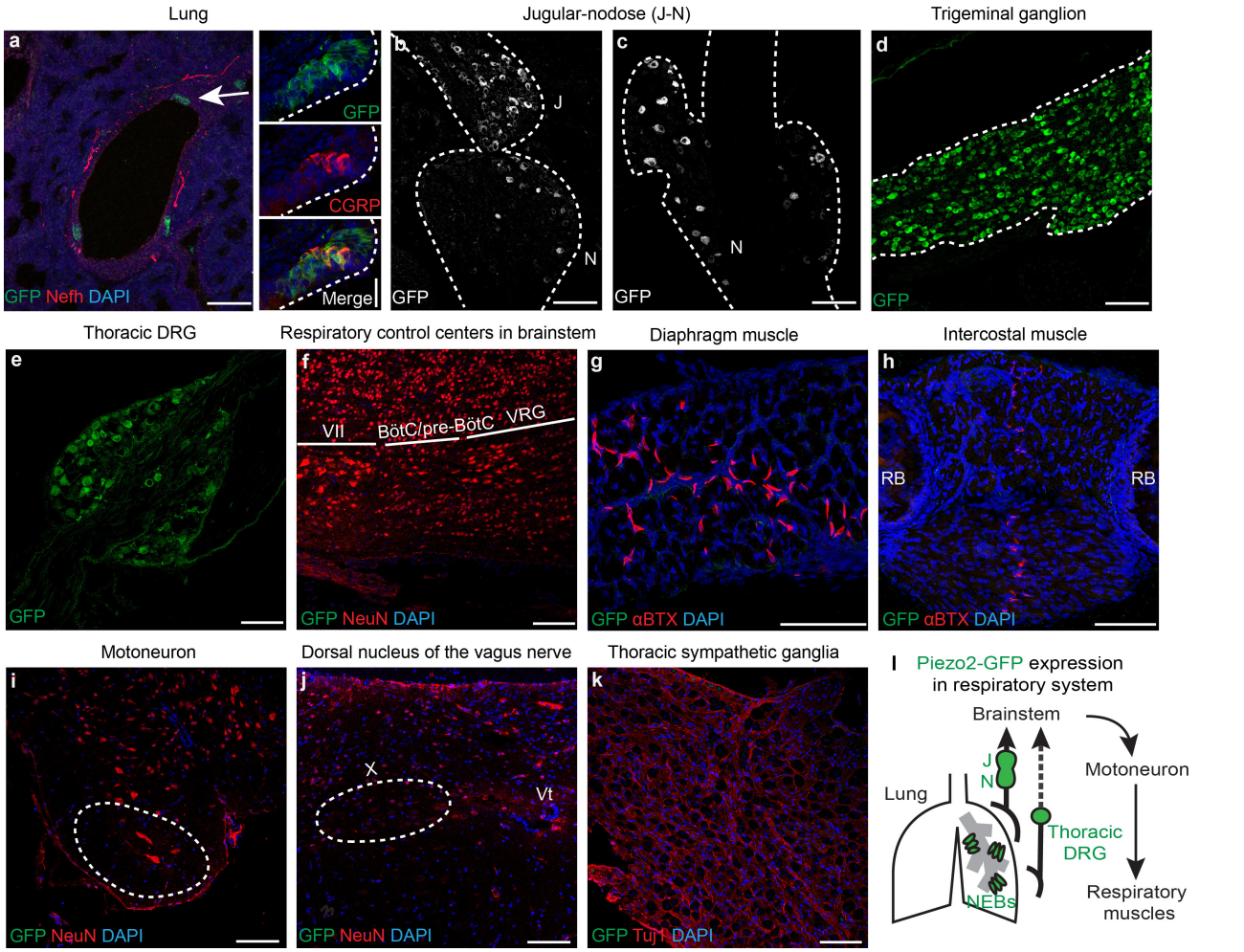

Extended Data Figure 2 | Piezo2 expression in the respiratory system. **a**, Co-immunostaining for GFP and Nefh in P0 *Piezo2*^{GFP} reporter lung. Arrow, NEB. Smaller panels on right show a magnified view of NEB stained for GFP and CGRP (a marker of NEBs). **b**, **c**, GFP immunostaining in the jugular–nodose complex from P0 (**b**) and adult (**c**) *Piezo2*^{GFP} reporter mice. Dotted line demarcates the boundary of the jugular–nodose complex. **d**, **e**, GFP immunostaining in P0 trigeminal ganglion (**d**) or adult thoracic DRG (**e**) from *Piezo2*^{GFP} reporter mice. Dotted line in (**d**) demarcates the boundary of the trigeminal ganglion. **f**, Co-immunostaining for GFP and NeuN in a sagittal section of P0 *Piezo2*^{GFP} brainstem. **g**, **h**, GFP and αBTX (a marker of neuromuscular junction) co-staining in P0 *Piezo2*^{GFP} diaphragm (**g**) and intercostal muscles (**h**). **i**, Co-immunostaining for GFP and NeuN in adult *Piezo2*^{GFP} lumbar spinal cord. Dotted circle indicates motor neuron localization. **j**, Co-immunostaining for GFP and NeuN in adult *Piezo2*^{GFP} brainstem. Dotted circle marks dorsal nucleus of the vagus nerve, X. **k**, Co-immunostaining for GFP and Tuj1 in thoracic sympathetic ganglia from adult *Piezo2*^{GFP} reporter mice. **l**, Schematic summary of Piezo2–GFP expression in the respiratory system. VII, facial nucleus; BötC, the Bötzinger complex; VRG, ventral respiratory group; RB, rib bone; Vt, ventricle. Scale bars, 20 μm (smaller panels on right in **a**), 100 μm (all other panels).

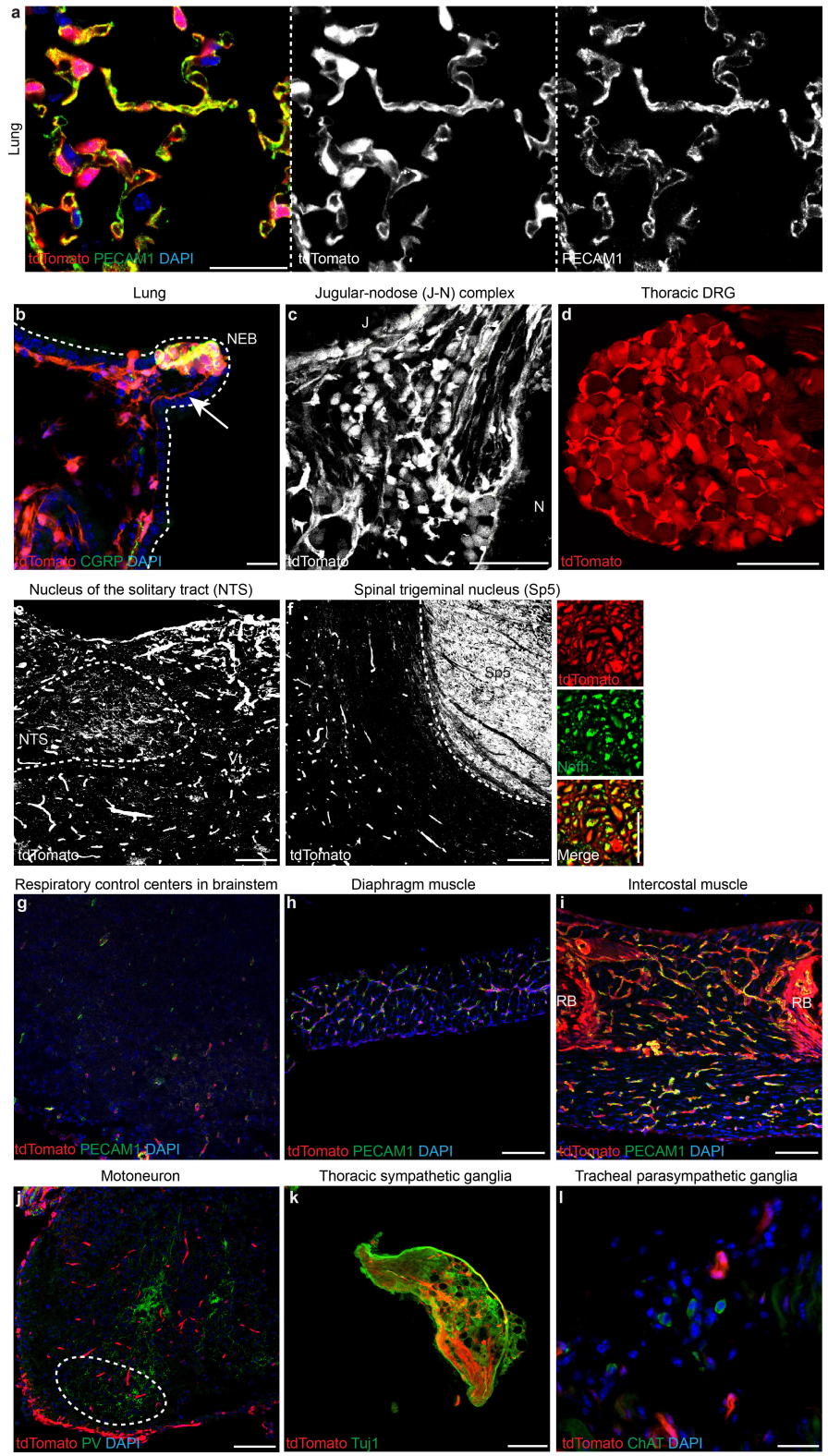

Extended Data Figure 3 | Characterization of tdTomato expression in the respiratory system of *Piezo2-GFP-IRES-Cre* (*Piezo2*^{GFP});*Ai9* reporter mice. a, **b**, Immunostaining for PECAM1 (**a**) and CGRP (**b**) with tdTomato epifluorescence in postnatal lungs. Arrow in (**b**) indicates tdTomato^{+} nerve fibre innervating NEB. Dotted line in (**b**) demarcates the lung epithelium. **c**, tdTomato epifluorescence in P0 jugular–nodose complex. Dotted line in (**c**) demarcates the boundary of the jugular–nodose complex. **d**, tdTomato epifluorescence in adult thoracic DRG. **e**, **f**, tdTomato epifluorescence in adult nucleus of the solitary tract (NTS) (**e**) and in adult spinal trigeminal nucleus (Sp5) (**f**), where axons of nodose and jugular/trigeminal sensory neurons project, respectively[52,53]. Smaller panels on right in **f** show a magnified view of Sp5 with Nefh staining. **g**–**i**, PECAM1 immunostaining with tdTomato epifluorescence in P0 brainstem (**g**), adult diaphragm (**h**), and P0 intercostal muscle (**i**). **j**, PV immunostaining with tdTomato epifluorescence in postnatal lumbar spinal cord. Dotted circle marks motor neuron localization. **k**, Tuj1 immunostaining with tdTomato epifluorescence in adult thoracic sympathetic ganglia. **l**, ChAT immunostaining and tdTomato epifluorescence in tracheal parasympathetic ganglia from adult reporter mice. Scale bars, 25 μm (**a**, **l**, smaller panels on right in **f**), 20 μm (**b**), 100 μm (**c**–**k**).

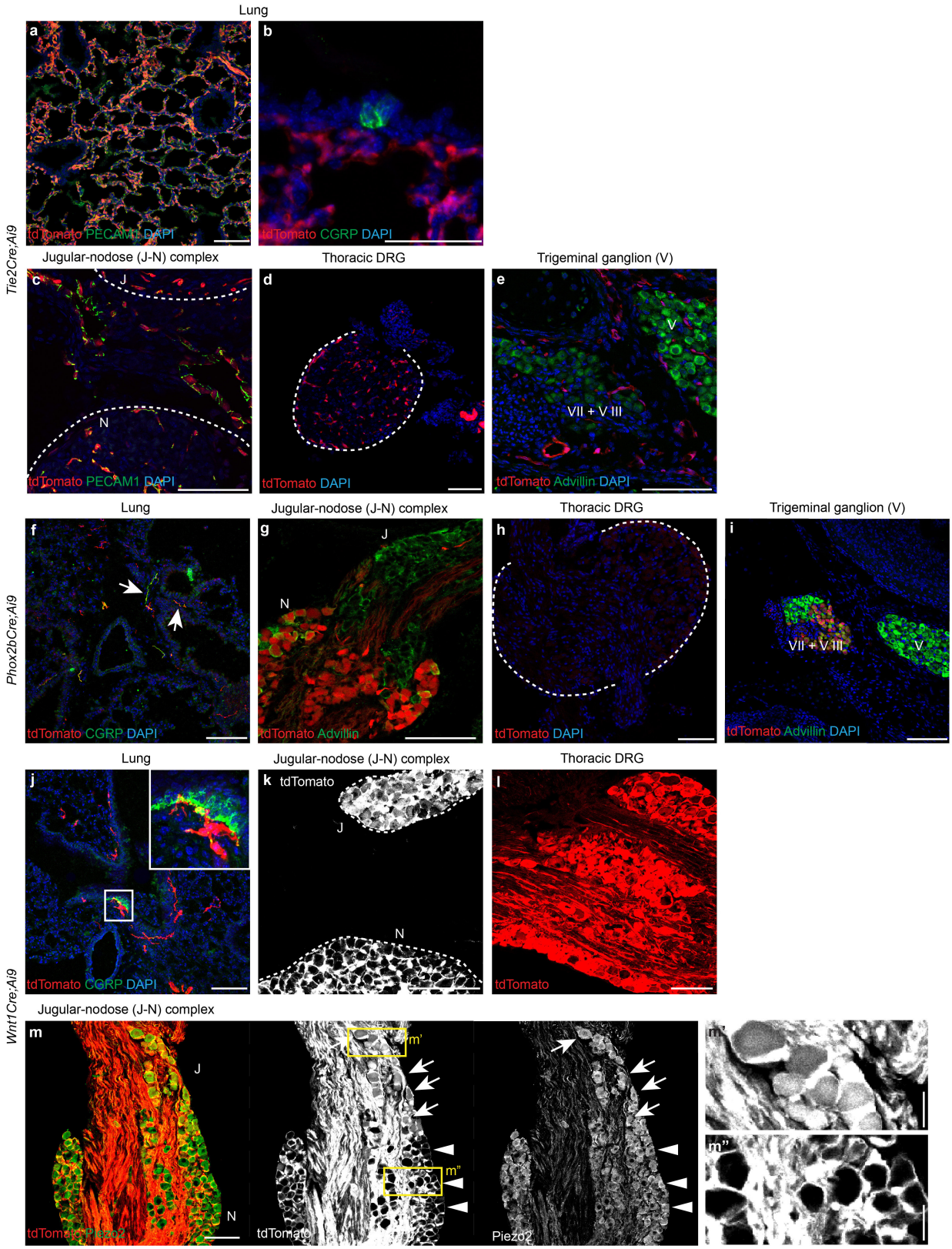

Extended Data Figure 4 | See next page for caption.

Extended Data Figure 4 | Characterization of tissue-specific Cre activities via *Ai9* reporters. a, **b**, tdTomato epifluorescence in P0 *Tie2Cre;Ai9* lung with PECAM1 staining (**a**) or CGRP staining (**b**). **c**, tdTomato epifluorescence in P0 *Tie2Cre;Ai9* jugular–nodose complex with PECAM1 staining. Dotted line demarcates the boundary of the jugular–nodose complex. **d**, tdTomato epifluorescence in adult *Tie2Cre;Ai9* thoracic DRG. Dotted line demarcates the boundary of the DRG. **e**, tdTomato epifluorescence in P0 *Tie2Cre;Ai9* trigeminal ganglion with Advillin staining. TdTomato signal co-localizes with PECAM1$^+$ endothelial cells in **a** and **c**. **f**–**i**, tdTomato epifluorescence in P0 *Phox2bCre;Ai9* lung with CGRP staining (**f**), P0 jugular–nodose complex with Advillin staining (**g**), adult thoracic DRG (**h**), and P0 trigeminal ganglion with Advillin staining (**i**). TdTomato signal is present in nodose ganglia (**g**), but absent in lung cells and NEBs (**f**), jugular ganglia (**g**), DRG (**h**), and trigeminal ganglia (**i**). Arrows in **f** indicate tdTomato$^+$ vagal nerve fibre innervating the lung epithelium. Dotted line in **h** demarcates the boundary of DRG. **j**–**m**, tdTomato epifluorescence in P0 *Wnt1Cre;Ai9* lung with CGRP staining (**j**), P0 jugular–nodose complex (**k**), adult thoracic DRG (**l**), and adult jugular–nodose complex with Piezo2 staining (**m**). **m′**, **m′′**, Higher magnification images of **m**. Arrows show tdTomato expression in both jugular neuronal cell bodies and satellite cells. Arrowheads show tdTomato expression only in satellite cells. TdTomato signal is present in neuronal cell bodies of jugular ganglia (**k**, **m**) and DRG (**l**), and satellite cells in the jugular–nodose complex and DRG (**k**–**m**), but absent in lung cells and NEBs (**j**) and neuronal cell bodies of nodose ganglia (**k**, **m**). TdTomato$^+$ nerve fibres innervate the lung (**j**). Dotted lines indicate boundaries of the ganglia. VII + VIII, facial-acoustic complex. Scale bars, 50 μm (**b**), 12.5 μm (**m′**, **m′′**), 100 μm (all other panels).

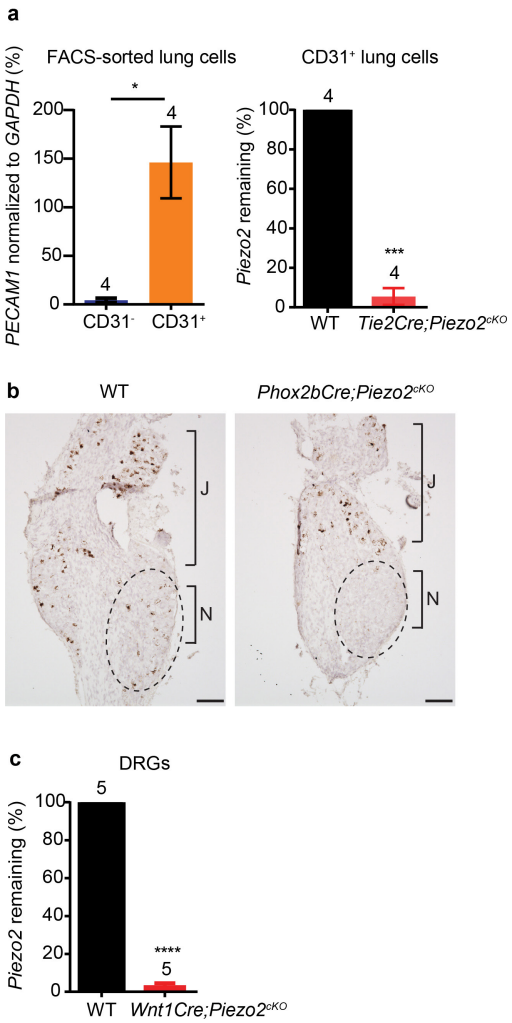

Extended Data Figure 5 | Characterization of Piezo2 knockdown in Piezo2 conditional knockout mice. a, Characterization of *Piezo2* knockdown by qRT–PCR using FACS-sorted CD31^{+} (or PECAM1^{+}) lung cells from adult wild-type and *Tie2Cre;Piezo2^{cKO}* mice. **b**, *Piezo2 in situ* hybridization in the jugular–nodose complex of adult wild-type and *Phox2bCre;Piezo2^{cKO}* mice. Dotted circles mark nodose ganglia (N). **c**, qRT–PCR using DRG isolated from P0 wild-type and *Wnt1Cre;Piezo2^{cKO}* pups. $*P < 0.05$, $***P < 0.001$, $****P < 0.0001$, unpaired Welch's *t*-test for **a**, **c**. Data are presented as mean ± s.e.m. Scale bar, 100 μm.

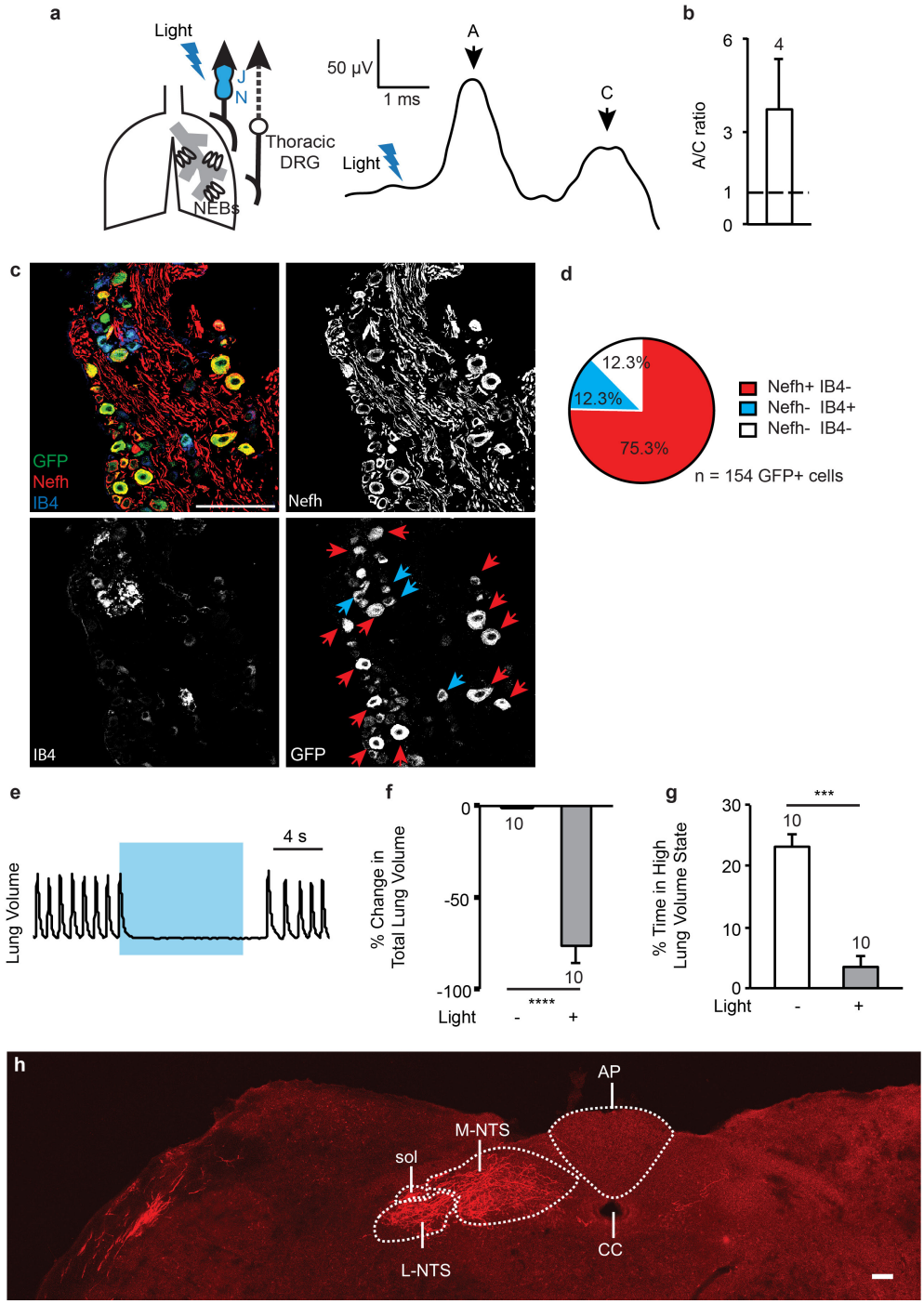

Extended Data Figure 6 | See next page for caption.

Extended Data Figure 6 | Optogenetic activation of Piezo2$^+$ vagal sensory neurons in *Piezo2^{GFP};lox-ChR2* mice. a, A compound action potential response following brief optogenetic stimulation (blue lightning sign) of vagus nerve in *Piezo2^{GFP};lox-ChR2* mice. **b**, A and C currents classified on the basis of corresponding peak area in the compound action potential. Dashed line: A–C ratio of 1. Data are presented as mean ± s.e.m. **c**, GFP, Nefh and IB4 co-staining in adult *Piezo2^{GFP}* jugular–nodose complex. Red arrows indicate GPF$^+$ Nefh$^+$ IB4$^-$ cells; blue arrows indicate GFP$^+$ Nefh$^-$ IB4$^+$ cells. **d**, Percentage of Nefh or IB4 positive cells among GFP$^+$ cells in adult *Piezo2^{GFP}* jugular–nodose complex. **e**–**g**, State of respiratory trapping following optogenetic stimulation (50 Hz, 10 s) of vagus nerve in *Piezo2^{GFP};lox-ChR2* mice. Representative trace showing changes in lung volume following optogenetic activation in *Piezo2^{GFP};lox-ChR2* mice (**e**). Per cent change in total lung volume in *Piezo2^{GFP};lox-ChR2* mice without and with light (**f**). The percentage of time in a high lung volume state (greater than mean volume during tidal breathing) in *Piezo2^{GFP};lox-ChR2* mice without and with light (**g**). $^{***}P < 0.001$, $^{****}P < 0.0001$, paired *t*-test, mean ± s.e.m. **h**, Brainstem of *Piezo2^{GFP}* mice with *AAV-flex-tdTomato* injection to the jugular–nodose complex. Sol, solitary tract; CC, central canal; AP, area postrema; L-NTS; ventral, lateral, ventrolateral, interstitial, and intermediate NTS subnuclei; M-NTS; dorsolateral, dorsomedial, medial, and commissural NTS subnuclei. Scale bars, 100 μm.

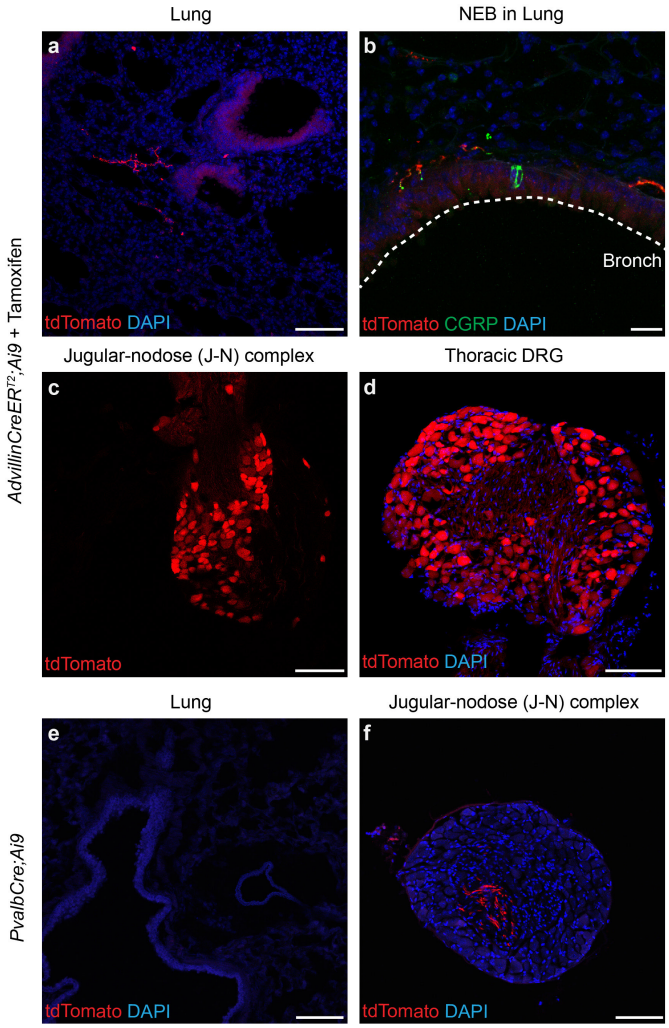

Extended Data Figure 7 | Characterization of AdvillinCreER^{T2} and PvalbCre activity via *Ai9* reporter. a, tdTomato epifluorescence and DAPI staining in the lung from adult *AdvillinCreER^{T2};Ai9* $^{+Tam}$ reporter mice. TdTomato is not expressed in lung cells. Instead, tdTomato^{+} nerve fibres innervate the lung. **b**, tdTomato epifluorescence, CGRP and DAPI staining in lungs from adult *AdvillinCreER^{T2};Ai9* $^{+Tam}$ reporter mice. TdTomato is not expressed in NEBs. Dotted line demarcates the lung epithelium. Bronch, bronchioles. **c**, **d**, tdTomato epifluorescence in adult jugular–nodose complex (**c**) and tdTomato epifluorescence and DAPI staining in adult thoracic DRG (**d**) from *AdvillinCreER^{T2};Ai9* $^{+Tam}$ reporter mice. TdTomato is expressed in both the jugular–nodose complex (**c**) and the DRG (**d**). **e**, **f**, tdTomato epifluorescence and DAPI staining in the lung (**e**) and jugular–nodose complex (**f**) of adult *PvalbCre;Ai9* reporter mice. TdTomato is not expressed in lung cells and neuronal cell bodies in the jugular–nodose complex. Scale bars, 100 μm.

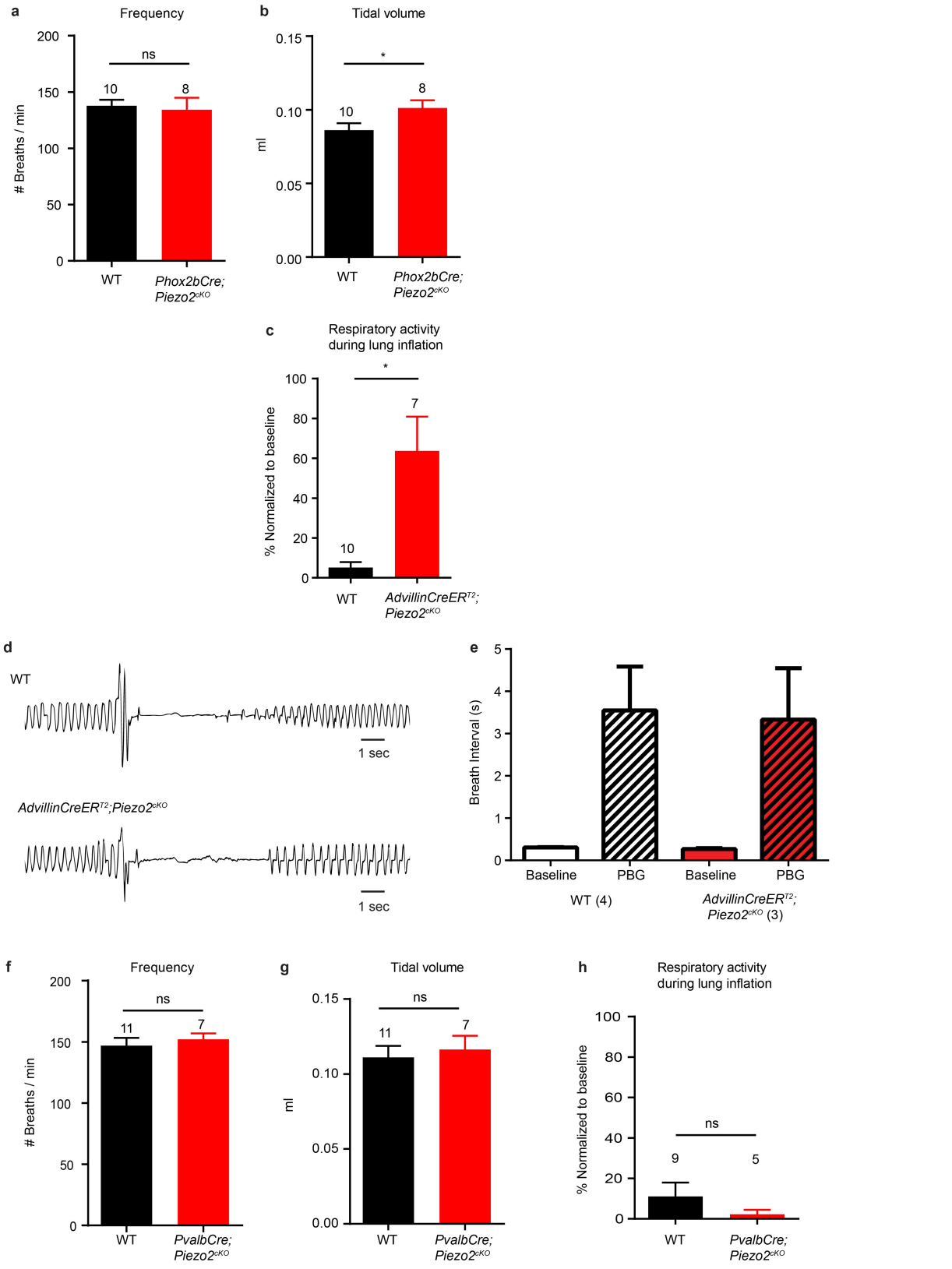

Extended Data Figure 8 | Respiratory properties of various *Piezo2*-deficient mouse lines. a, **b**, Average frequency (**a**) and average tidal volume (**b**) of adult wild-type and *Phox2bCre;Piezo2*^{cKO} mice under anaesthesia. *$P < 0.05$, unpaired Student's *t*-test, mean ± s.e.m. **c**, Respiration activity during lung inflation (0.3 ml air) normalized to baseline in adult wild-type and *AdvillinCreER*^{T2}*;Piezo2*^{cKO} mice. *$P < 0.05$, unpaired Welch's *t*-test, mean ± s.e.m. **d**, **e**, Phenylbiguanide (PBG)-induced chemoreflex in adult *AdvillinCreER*^{T2}*;Piezo2*^{cKO} mice. Representative traces of respiratory air flow from wild-type and *AdvillinCreER*^{T2}*;Piezo2*^{cKO} mice with 2.0 μg PBG intravenous injection (**d**). Baseline and longest breath interval after PBG injection. Bars represent mean ± s.e.m. (**e**). **f**, **g**, Average frequency (**f**) and average tidal volume (**g**) of adult wild-type and *PvalbCre;Piezo2*^{cKO} mice under anaesthesia. Unpaired Student's *t*-test, mean ± s.e.m. **h**, Respiration activity during lung inflation (0.3 ml air) normalized to baseline in adult wild-type and *PvalbCre;Piezo2*^{cKO} mice. Unpaired Welch's *t*-test, mean ± s.e.m. NS, statistically not significant.

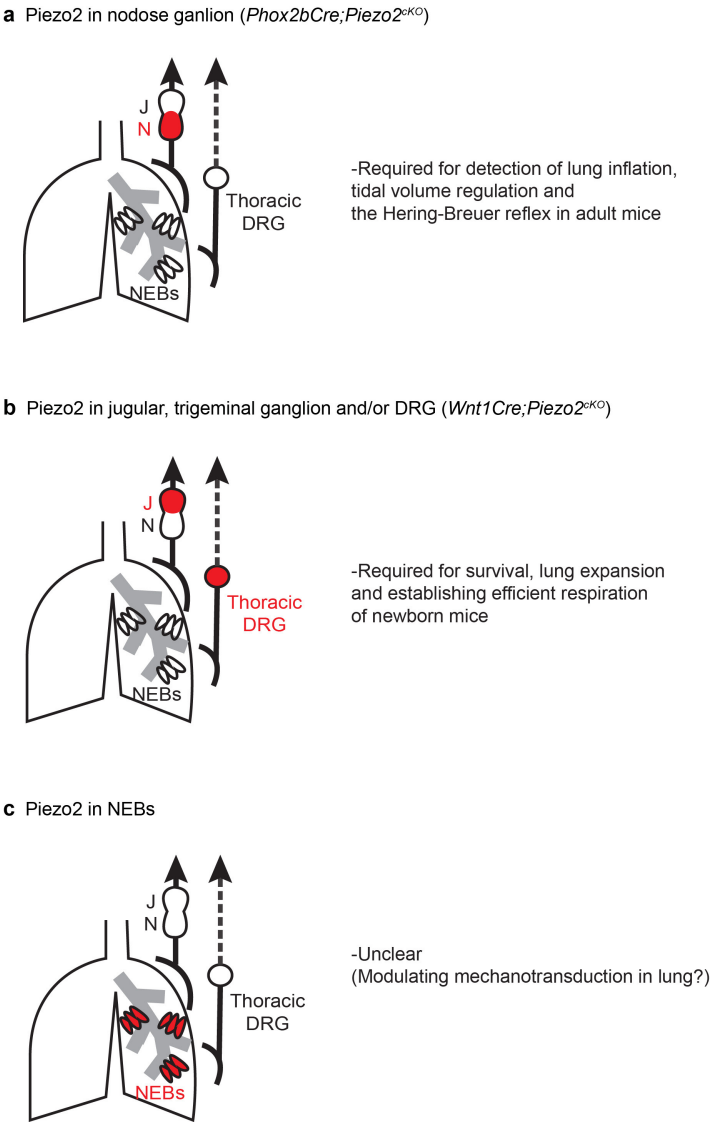

Extended Data Figure 9 | Roles of Piezo2 in respiratory system. **a**, Piezo2 in nodose sensory neurons. It has been widely reported that nodose sensory neurons contain low-threshold mechanosensors innervating the lower airway tract including the lungs, while jugular sensory neurons contain high-threshold mechanosensors that innervate the upper airway tract, such as the larynx and the trachea. In addition, nodose sensory neurons project to the NTS[6,53], a synaptic station required for the Hering–Breuer reflex in the brainstem[54]. Consistent with these findings, Piezo2 expression is detected in the jugular–nodose ganglia complex, and Piezo2$^+$ nerve fibres project to the NTS. Moreover, adult mice lacking Piezo2 in the nodose ganglion show abolished vagal nerve responses to lung inflation, increased tidal volume, and an impaired Hering–Breuer inspiratory reflex. In addition to the nodose ganglia, Piezo2 is also expressed in the jugular, trigeminal, and dorsal root ganglia. We observed similar phenotypes in mice with Piezo2 depletion induced in virtually all sensory neurons in the adult. These data suggest that Piezo2 in nodose sensory neurons is the major stretch sensor required for lung volume regulation and the Hering–Breuer reflex response in adult mice. **b**, Piezo2 in jugular, trigeminal and/or spinal sensory neurons. In newborn mice, Piezo2 in sensory neurons of the neural crest origin is required for proper lung expansion and establishing efficient respiration as both global Piezo2 knockout and neural crest-derived sensory neuron-specific Piezo2 conditional knockout newborn mice showed hypoventilation, decreased inspiratory activity, altered expiratory pattern and unexpanded lungs. Our genetic studies also suggest that Piezo2 is not required in nodose ganglia for newborn lung expansion and respiration; however, this lack of requirement does not imply lack of involvement, and could be due to functional redundancy (that is, Piezo2 in jugular, trigeminal and/or dorsal root ganglia can compensate for Piezo2 deficiency in nodose ganglia). Although sensory neuronal control of respiration in newborn animals remains largely unknown, the newborn airway experiences a large pressure change in the course of lung expansion[55]. Piezo2-mediated mechanosensory feedback of the airway might be crucial for subsequent motor output (for example, control of diaphragm discharge or prevention of upper airway narrowing) to establish proper breathing patterns in newborn animals. The data presented here do not identify the exact cause of lethality in Piezo2-deficient newborn animals; however, we speculate that lethality in pups might be due to a combined effect of hypoventilation and lack of nutrients owing to inability to suckle. **c**, Piezo2 in NEBs. In addition to airway-innervating sensory neurons, Piezo2 is also expressed in pulmonary NEB cells, which are likely to be innervated by Piezo2$^+$ afferents (Extended Data Fig. 3b, arrow). NEBs are enigmatic pulmonary cells whose physiological function is unclear[3,22,23]. Previous studies have suggested that the inflation-induced vagal nerve responses that are responsible for the Hering–Breuer reflex are slowly adapting[2,4,5,7]. While Piezo2 channels are generally rapidly adapting when assayed in cultured cells[16], Piezo2 channels in Merkel cell–neurite complexes in the skin give rise to slowly adapting firing responses[21,56] that are proposed to be caused by dual Piezo2 expression in both epidermal Merkel cells and associated afferents[21,56]. Therefore, it is possible that NEBs also contribute to sensing lung inflation in concert with Piezo2$^+$ mechanosensory afferents. Future efforts will explore whether pulmonary NEBs function as mechanosensory cells, similar to Merkel cells.

Extended Data Table 1 | Respiratory properties of anaesthetized wild-type and *AdvillinCreER^{T2};Piezo2^{cKO}* mice

Parameter	Abbreviation	Unit	Definition	*p* value	WT average ± SEM	cKO average ± SEM
Frequency	f	breaths/min	Number of breaths per minute	0.5939 (W)	144.5 ± 3.167	149.8 ± 8.894
Tidal Volume per breath	TVb	ml	Volume of air per breath	0.0143 (S)	0.1002 ± 0.006839	0.1310 ± 0.008891
Minute Volume	MVb	ml/min	f x TVb	0.0727 (W)	14.38 ± 0.9114	19.84 ± 2.460
Inspiratory Time	Ti	sec	Actual time of inspiration	0.4727 (S)	0.1506 ± 0.006858	0.1588 ± 0.008984
Expiratory Time	Te	sec	Actual time of expiration	0.4135 (S)	0.2694 ± 0.008343	0.2550 ± 0.01618
Rpef	Rpef	-	Rate to achieve peak expiratory flow Rpef=(time to PEF)/Te	0.0221 (S)	0.1131 ± 0.00687	0.1461 ± 0.01160
Peak Inspiratory Flow	PIFb	ml/sec	Peak airflow velocity during inspiration	0.2112 (S)	1.173 ± 0.1251	1.471 ± 0.2021
Peak Expiratory Flow	PEFb	ml/sec	Peak airflow velocity during expiration	0.6118 (S)	1.519 ± 0.1381	1.635 ± 0.1824
Expiratory Flow at 50% Volume	EF50	ml/sec	Airflow at when 50% of tidal volume is expired	0.3153 (S)	0.1002 ± 0.01059	0.1182 ± 0.01407
Relaxation Time[58]	Tr	sec	Time for the volume signal to reach 36% of the peak amplitude during expiration	0.1363 (S)	0.06248 ± 0.004801	0.07562 ± 0.007158
Pause[58]	PAU	-	(Te-Tr)/Tr	0.1755 (S)	3.660 ± 0.3798	2.790 ± 0.4899
Enhanced Pause[57]	Penh	-	PEFb/PIFb x PAU	0.4161 (S)	5.392 ± 0.5581	4.339 ± 1.241
Duration of Breaking[57]	TB	%	The percentage of time occupied by the top of the breath (at or near tidal volume)	0.1526 (S)	3.579 ± 0.5614	4.782 ± 0.5386
Duration of Pause before Inspiration[57]	TP	%	The percentage of time occupied by the bottom of the breath (at or near functional residual capacity).	0.0800 (S)	45.65 ± 2.297	37.86 ± 3.651

Respiratory properties measured in wild-type ($n = 9$) and *AdvillinCreER^{T2};Piezo2^{cKO}* ($n = 7$) mice during plethysmograph recordings under anaesthesia (unpaired Student's (S) or Welch's (W) *t*-test)[57,58].